iScience

CellPress
OPEN ACCESS

Article

Latent CSN-CRL complexes are crucial for curcumin-induced apoptosis and recruited during adipogenesis to lipid droplets via small GTPase RAB18

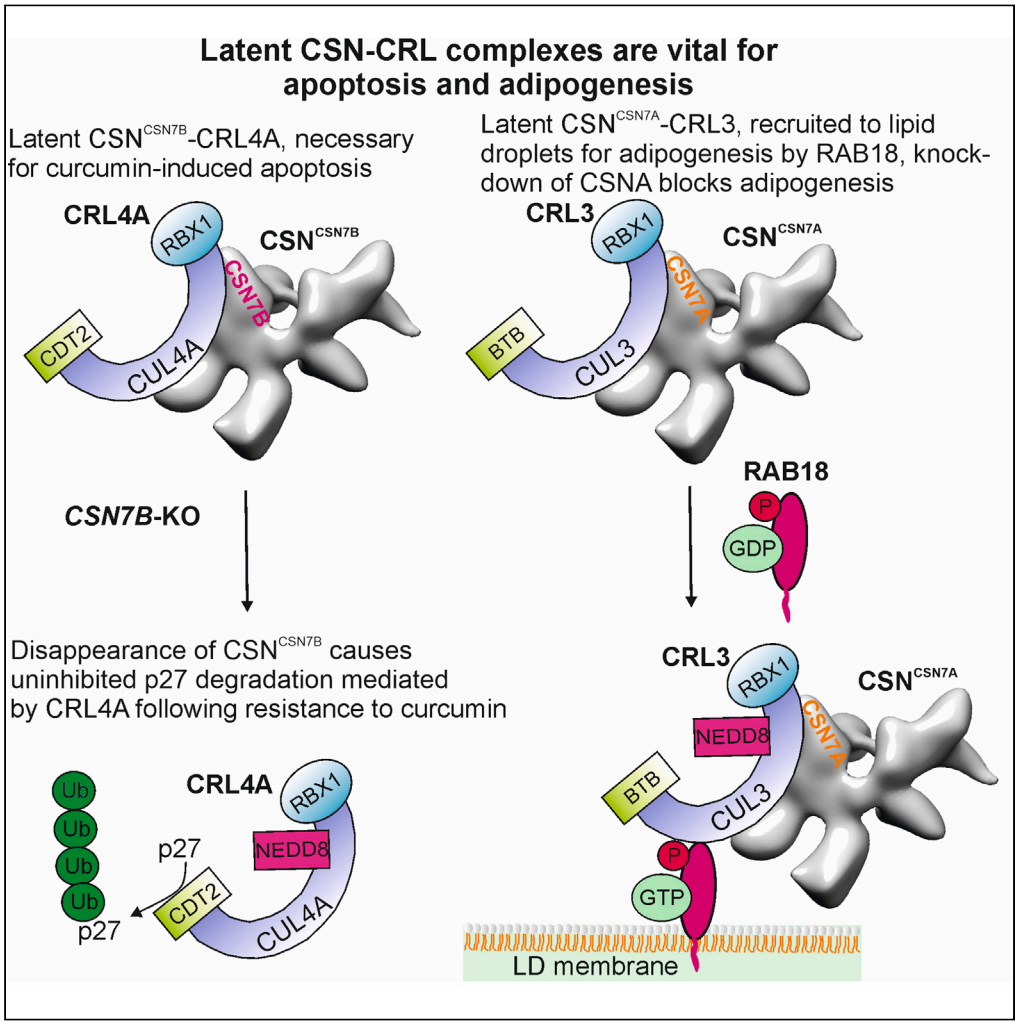

Dawadschargal Dubiel, Jing Wang, Roland Hartig, Supattra Chaithongyot, Wolfgang Dubiel, Michael Naumann

ddubiel@med.ovgu.de (D.D.)
wolfgang.dubiel@med.ovgu.de (W.D.)

Highlights

The variant CSN^CSN7A preferentially binds to CRL3, and CSN^CSN7B, to CRL4A/B

Latent CSN^CSN7A-CRL3 and latent CSN^CSN7B-CRL4A/B complexes occur in cells

Curcumin-induced apoptotic cell death requires latent CSN^CSN7B-CRL4A

RAB18 recruits latent CSN^CSN7A-CRL3 to lipid droplets during adipogenesis

Dubiel et al., iScience 26, 106468
April 21, 2023
https://doi.org/10.1016/j.isci.2023.106468

iScience

CellPress
OPEN ACCESS

Article

Latent CSN-CRL complexes are crucial for curcumin-induced apoptosis and recruited during adipogenesis to lipid droplets via small GTPase RAB18

Dawadschargal Dubiel,[1,*] Jing Wang,[2] Roland Hartig,[3] Supattra Chaithongyot,[1] Wolfgang Dubiel,[1,2,4,*] and Michael Naumann[1]

SUMMARY

The COP9 signalosome (CSN) and cullin-RING ubiquitin ligases (CRLs) form latent CSN-CRL complexes detectable in cells. We demonstrate that the CSN variants CSN^{CSN7A} and CSN^{CSN7B} preferentially bind to CRL3 or CRL4A and CRL4B, respectively. Interestingly, the interacting protein ubiquitin-specific protease 15 exclusively binds to latent CSN^{CSN7A}-CRL3, while $p27^{KIP}$ attaches to latent CSN^{CSN7B}-CRL4A complex. Inhibition of deneddylation by CSN5i-3 or neddylation by MLN4924 do not impede the formation of latent complexes. Latent CSN^{CSN7A}-CRL3 and latent CSN^{CSN7B}-CRL4A/B particles are essential for specific cellular functions. We found that curcumin-induced cell death requires latent CSN^{CSN7B}-CRL4A. Knockout of *CSN7B* in HeLa cells leads to resistance against curcumin. Remarkably, the small GTPase RAB18 recruits latent CSN^{CSN7A}-CRL3 complex to lipid droplets (LDs), where CRL3 is activated by neddylation, an essential event for LD formation during adipogenesis. Knockdown of CSN7A or RAB18 or destabilization of latent complexes by cutting off CSN7A C-terminal 201–275 amino acids blocks adipogenesis.

INTRODUCTION

Mammalian COP9 signalosome (CSN) consists of eight core subunits,[1] CSN1 to CSN8, characterized either by the proteasome lid-CSN-initiation factor 3 (PCI) domain (CSN1-CSN4, CSN7, and CSN8) or by the MPR1/PAD1 N-terminal (MPN) domain (CSN5 and CSN6).[2] PCI domains form an open ring[3] resulting in a horseshoe-shaped structure.[4] The C termini from each subunit constitute the helical bundle (HB), whereas CSN5 and CSN6 assemble as a heterodimer sitting on top of the HB.[3] Interestingly, similar architecture is shared by the CSN paralog complexes, the 26S proteasome lid, and the eukaryotic initiation factor 3.[3]

The CSN forms complexes with cullin-RING ubiquitin ligases (CRLs).[3,5,6] As shown for CSN-CRL4A *in vitro*, CSN2 contacts with CUL4A C terminus, CSN2 and CSN4 bind to RBX1, and CSN1 interacts with DDB1. Binding leads to conformational changes of CSN2, CSN4, and CSN7 moving CSN5-CSN6 dimer and inducing CSN5 for deneddylation activity.[5,7,8] The CSN is a deubiquitylating enzyme (DUB) complex,[9] which hydrolyzes via CSN5-MPN+/JAMM domain NEDD8 from cullins (cullin 1-9, CUL1-9).[3,5,6] Removal of NEDD8 inactivates CRLs and protects them from autoubiquitylation.[10] It allows the exchange of substrate receptors (SRs) using CAND1 as SR exchange factor[11] to prepare CRLs for adaptation to fluctuations in substrate availability.[11–13]

Largely overlooked is the fact that the CSN is more heterogeneous than indicated by the structure of the 8-subunit complex. It has been recognized that a fraction of the cellular CSN contains a non-canonical subunit.[14,15] In addition, CSNs are associated with diverse DUBs forming multi-DUB complexes.[9] Moreover, CSNs interact with $p27^{KIP}$ (p27)[16] or rat sarcoma (RAS)-related, small GTPase 18 (RAB18),[17] proteins involved in apoptotic cell death and adipogenesis. A further unexplored source of heterogeneity is provided by the fact that several CSN subunits occur as paralogs. Human CSN7 is encoded by two related genes, *COPS7A/CSN7A* and *COPS7B/CSN7B*, forming CSN variants. In Mammalia, CSN^{CSN7A} and CSN^{CSN7B} variants co-exist, but their individual functions are largely unknown.

[1]Institute of Experimental Internal Medicine, Medical Faculty, Otto von Guericke University, Leipziger Str. 44, 39120 Magdeburg, Germany

[2]School of Pharmaceutical Sciences, State Key Laboratory of Cellular Stress Biology, Fujian Provincial Key Laboratory of Innovative Drug Target Research, Xiamen University, Xiang'an South Road, Xiamen 361102 Fujian, China

[3]Multi-Parametric Bioimaging and Cytometry Unit (Confocal Microscopy & Flow Cytometry), Institute of Molecular and Clinical Immunology, Medical Faculty, Otto von Guericke University, Leipziger Str. 44, 39120 Magdeburg, Germany

[4]Lead contact

*Correspondence: ddubiel@med.ovgu.de (D.D.), wolfgang.dubiel@med.ovgu.de (W.D.)

https://doi.org/10.1016/j.isci.2023.106468

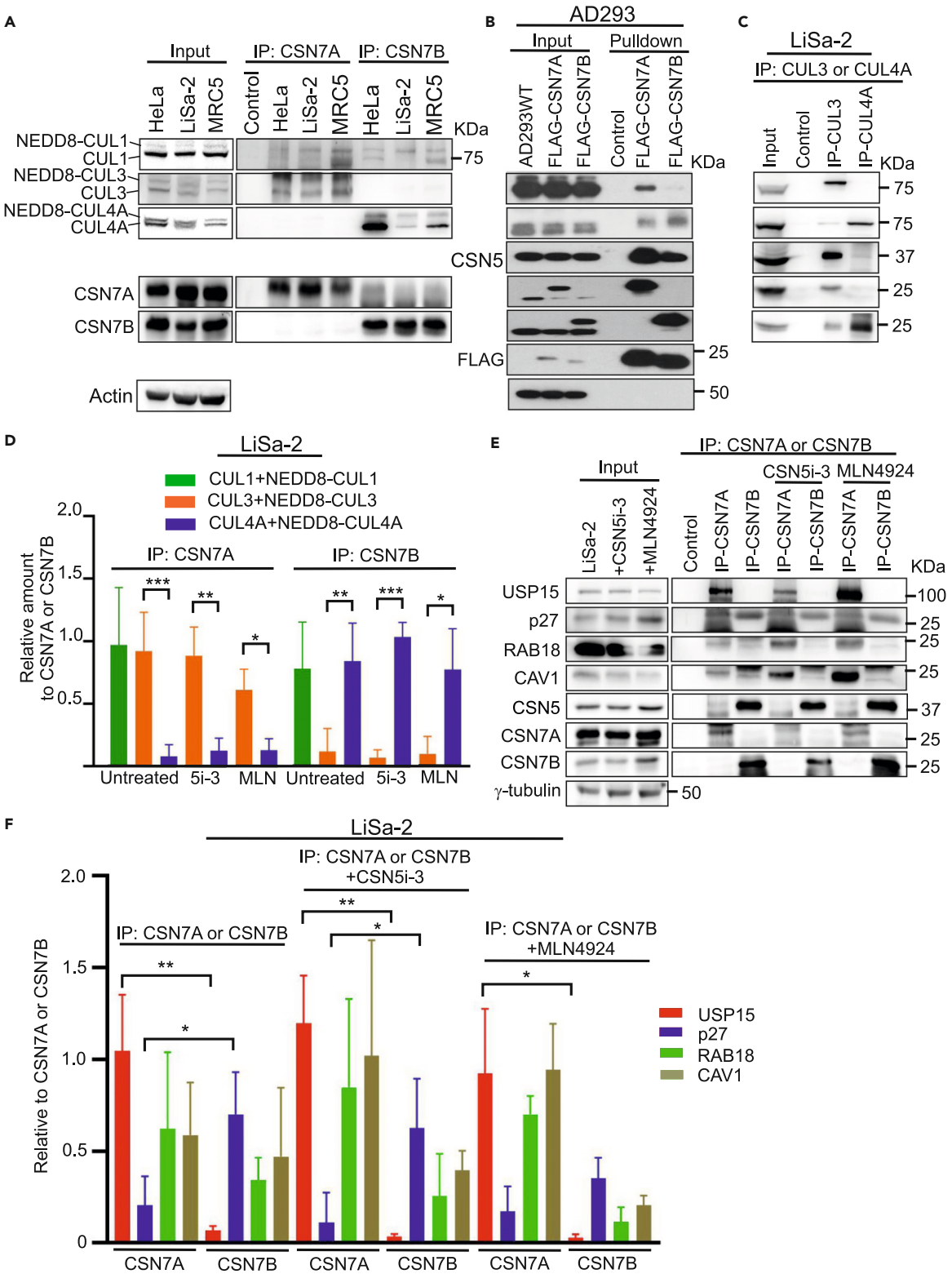

Figure 1. Preferential binding of CSN7A to CUL3 and CSN7B to CUL4A and specific interactions of USP15, p27, RAB18, and CAV1 with CSN7A and CSN7B

(A) HeLa, LiSa-2, and MRC5 cell lysates were immunoblotted (Input). Immunoprecipitates of CSN7A or CSN7B were analyzed by indicated antibodies. Control was performed with non-immunized serum from rabbit (Control).

Figure 1. *Continued*

(B) AD293WT, AD293-FLAG-CSN7A, and AD293-FLAG-CSN7B cell lysates were immunoblotted (Input). Pull-downs of FLAG-CSN7A and FLAG-CSN7B were analyzed by indicated antibodies. Empty FLAG-vector stably transfected into AD293 cells was used as control.

(C) LiSa-2 cell lysates were immunoblotted (Input). Immunoprecipitates of anti-CUL3 and anti-CUL4A antibodies were analyzed by indicated antibodies. Control was performed with non-immunized serum from rabbit (Control).

(D) Blots of LiSa-2 cells shown in (A) or in (S1A) were quantified by densitometry to determine the relative amounts of CUL1, CUL3, and CUL4A which were divided by relative amounts of immunoprecipitated CSN7A or CSN7B. Data are expressed as ratios of relative amounts of CUL1, CUL3, and CUL4A divided by relative amounts of CSN7A or CSN7B plus/minus standard deviations (SD, n = 3–5). Unpaired Student's t-test was used for statistical analysis. *$p < 0.05$, **$p < 0.01$, ***$p < 0.001$.

(E) LiSa-2 cells were incubated without or with CSN5i-3 (1 μM) or MLN4924 (1 μM) for 24 h, and then lysates were immunoblotted (Input). After incubation, immunoprecipitates of CSN7A or CSN7B were analyzed by indicated antibodies. Control was performed with non-immunized serum from rabbit (Control).

(F) Blots of LiSa-2 cells as shown in (E) were quantified by densitometry to determine the relative amounts of USP15, p27, RAB18, and CAV1 in the precipitates which were divided by the relative amounts of immunoprecipitated CSN7A or CSN7B. Data are expressed as ratios of relative amounts of USP15, p27, RAB18, and CAV1 divided by relative amounts of CSN7A or CSN7B plus/minus standard deviations (SD, n = 3). Unpaired Student's t-test was used for statistical analysis. *$p < 0.05$, **$p < 0.01$.

Interestingly, large amounts of inactive CSN-CRL complexes have been detected in cells. Nearly 30% of CUL1 and more than 40% of CUL4B are stably bound to CSN in 293T cells.[18] The role of **latent CSN-CRL complexes**, how we call the particles, remained unclear.[7,8,19] Here we demonstrate the significance of latent CSN-CRL complexes in apoptotic cell death and in adipogenesis. We show preferential binding of CSN^{CSN7A} to CRL3 and of CSN^{CSN7B} to CRL4A/B forming specific latent CSN-CRL complexes. Based on the known CSN interactome, we investigated the interactions of ubiquitin-specific protease 15 (USP15), p27, RAB18, and caveolin 1 (CAV1) with latent CSN^{CSN7A}-CRL3 and CSN^{CSN7B}-CRL4A/B complexes. We demonstrate that curcumin-mediated apoptosis needs latent CSN^{CSN7B}-CRL4A complex in HeLa cells and that RAB18 recruits latent CSN^{CSN7A}-CRL3 for lipid droplet formation during adipogenesis in LiSa-2 cells. By cutting off the C-terminal 201-stop amino acids of CSN7A and of CSN7B, interactions with CUL3 and CUL4A, respectively, were abolished, leading to disturbed apoptosis and adipogenesis.

RESULTS

CSN^{CSN7A} preferentially binds to CRL3, and CSN^{CSN7B}, to CRL4A/B complexes

Most prominent interacting protein complexes of CSN^{CSN7A} and CSN^{CSN7B} variants are CRLs. With respect to cullin deneddylation, knockout (KO) of one CSN7 paralog was largely compensated for by the other as shown in HeLa and AD293 cells.[20] Nevertheless, CSN variants prefer to bind specific CRLs. To obtain stable CSN-CRL complexes, we used single-detergent buffer (1% [v/v] Triton X-100) for cell lysis.[17] As shown in Figures 1A and S1A, immunoprecipitations of CSN7A or CSN7B co-precipitated CUL1 equally in HeLa and LiSa-2 as well as MRC5 cells. In contrast, mostly CUL3 was co-immunoprecipitated by CSN7A, and CUL4A, by CSN7B (Figure 1A). Equivalent results were obtained by FLAG pull-downs (Figure 1B). In stable transfected AD293 cells, integrated FLAG-CSN7A or FLAG-CSN7B were pulled down. Western blot analysis revealed a co-pull-down of CUL3 but less CUL4A with FLAG-CSN7A, whereas CUL4A was exclusively co-precipitated by FLAG-CSN7B. Moreover, immunoprecipitation of CUL3 in LiSa-2 cells co-precipitated mostly CSN7A, whereas CUL4A as well as CUL4B mostly co-precipitated with CSN7B (Figures 1C and S1B). The following experiments were conducted with CUL4A antibody.

We analyzed the impact of the chemical compounds CSN5i-3 (1 μM), a specific inhibitor of CSN-mediated deneddylation,[21] and the neddylation inhibitor MLN4924 (1 μM)[22,23] on binding of CSN^{CSN7A} and CSN^{CSN7B} variants to cullins. Although treatment with CSN5i-3 for 24 h completely blocks CUL3 and CUL4A deneddylation and MLN4924 inhibited CUL3 or CUL4A neddylation,[20] the two inhibitors had little or no influence on the preferential binding of CSN7A to CUL3 or CSN7B to CUL4A (Figure S1A). In Figure 1D, data of three separate experiments obtained with immunoprecipitations of CSN7A and CSN7B in LiSa-2 cells were quantified. It demonstrates similar co-precipitation of CUL1 with both CSN7A and CSN7B. On the other hand, CSN7A co-precipitated significantly more CUL3, whereas CSN7B was typically associated with CUL4A. We concluded that the inhibitors CSN5i-3 or MLN4924 had little or no impact on the interactions of CSN^{CSN7A} and CSN^{CSN7B} variants with CRL1 and preferential interactions of CSN^{CSN7A} with CRL3 or of CSN^{CSN7B} with CRL4A complexes. In other words, neddylation/deneddylation did not influence the formation of latent CSN^{CSN7A}/CSN^{CSN7B}-CRL1 and of CSN^{CSN7A}-CRL3 or CSN^{CSN7B}-CRL4A complexes under used conditions.

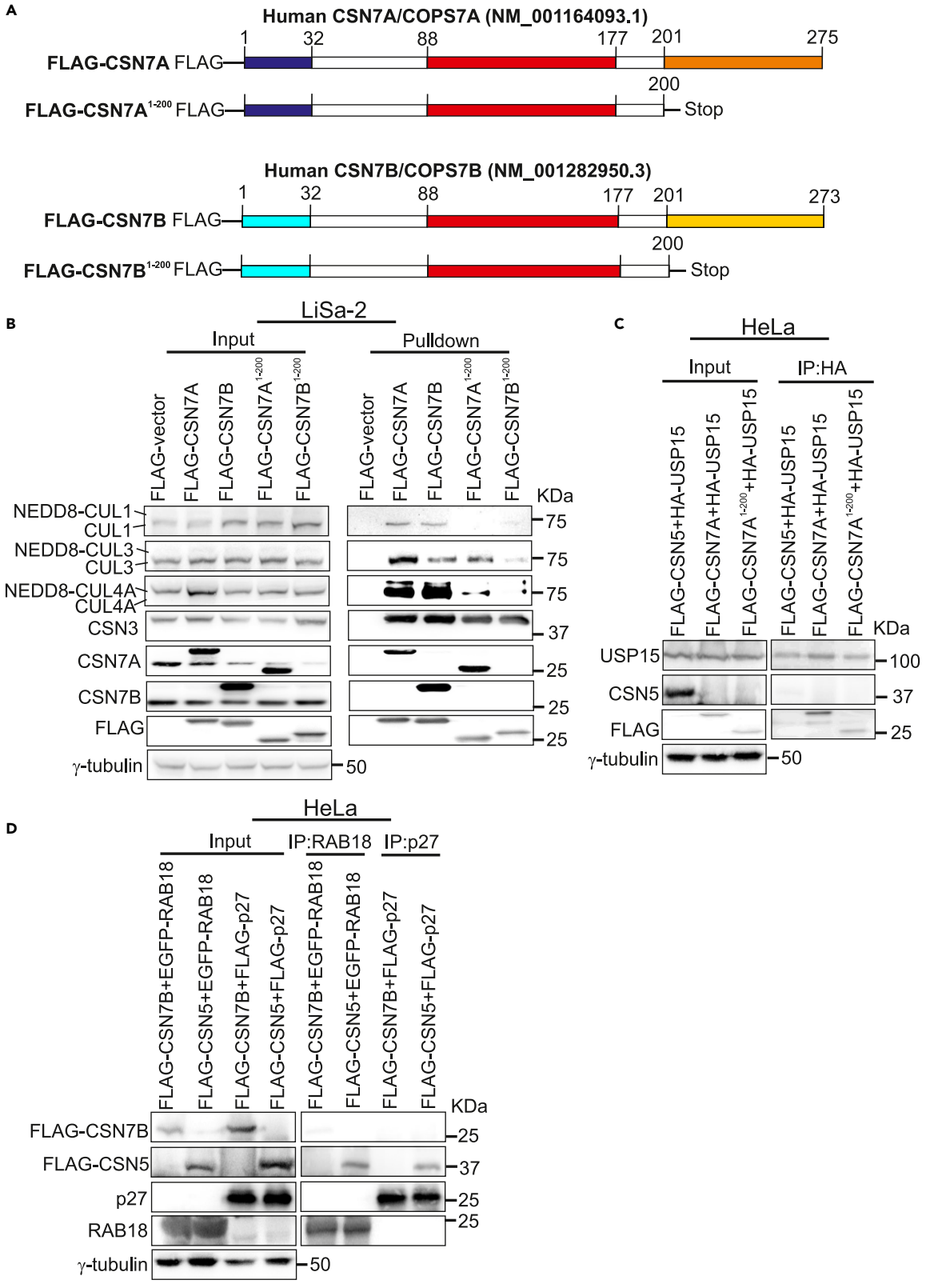
A
Human CSN7A/COPS7A (NM_001164093.1)
1
32
88
177
201
275
FLAG-CSN7A FLAG
200
FLAG-CSN7A1-200 FLAG
Stop
Human CSN7B/COPS7B (NM_001282950.3)
1
32
88
177
201
273
FLAG-CSN7B FLAG
200
FLAG-CSN7B1-200 FLAG
Stop
B
LiSa-2
Input
Pulldown
FLAG-vector
FLAG-CSN7A
FLAG-CSN7B
FLAG-CSN7A1-200
FLAG-CSN7B1-200
KDa
NEDD8-CUL1
CUL1
NEDD8-CUL3
CUL3
NEDD8-CUL4A
CUL4A
CSN3
CSN7A
CSN7B
FLAG
γ-tubulin
75
75
75
37
25
25
25
50
C
HeLa
Input
IP:HA
FLAG-CSN5+HA-USP15
FLAG-CSN7A+HA-USP15
FLAG-CSN7A1-200+HA-USP15
KDa
USP15
CSN5
FLAG
γ-tubulin
100
37
25
50
D
HeLa
Input
IP:RAB18
IP:p27
FLAG-CSN7B+EGFP-RAB18
FLAG-CSN5+EGFP-RAB18
FLAG-CSN7B+FLAG-p27
FLAG-CSN5+FLAG-p27
KDa
FLAG-CSN7B
FLAG-CSN5
p27
RAB18
γ-tubulin
25
37
25
25
50

Figure 2. Main CSN7A and CSN7B domains and relevance of their C-terminal 201-stop amino acids for selected protein-protein interactions

(A) Amino acid structure of human CSN7A/COPS7A (NM_001164093.1) and CSN7B/COPS7B (NM_001282950.3). The unique N-terminal 1–32 amino acids (blue) and C-terminal 201-stop amino acids (orange) and the homologous PCI domain (88–177 amino acids, red) are marked. FLAG-CSN7A$^{1\text{-}200}$ and FLAG-CSN7B$^{1\text{-}200}$ were used in further experiments.

(B) LiSa-2-FLAG-vector, LiSa-2-FLAG-CSN7A, LiSa-2-FLAG-CSN7B, LiSa-2-FLAG-CSN7A$^{1\text{-}200}$, and LiSa-2-FLAG-CSN7B$^{1\text{-}200}$ cell lysates were immunoblotted and analyzed with indicated antibodies. Additional bands seen in CSN7A and CSN7B are wild-type subunits (Input). FLAG pull-downs were performed, and FLAG-eluates were probed with the same antibodies. Empty FLAG-vector stably transfected into LiSa-2 cells was used as control. Since anti-CSN7B antibody has its epitope in the 201–273 amino acid region, it does not recognize FLAG-CSN7B$^{1\text{-}200}$.

(C) In HeLa cells, HA-USP15 was co-transfected with FLAG-CSN5, FLAG-CSN7A, or FLAG-CSN7A$^{1\text{-}200}$. After 16 h, immunoblots were analyzed with indicated antibodies (Input). At the same time, immunoprecipitations were performed with anti-HA antibody (IP: HA). Precipitates were evaluated with the same antibodies.

(D) In HeLa cells, FLAG-CSN7B and EGFP-RAB18 or FLAG-CSN5 and EGFP-RAB18 as well as FLAG-CSN7B and FLAG-p27 or FLAG-CSN5 and FLAG-p27 were co-transfected (Input). After 16 h, immunoblots were analyzed with indicated antibodies (Input). In parallel, immunoprecipitations were performed with anti-RAB18 or -p27 antibodies. Precipitates were evaluated with the same antibodies (IP: RAB18 and IP: p27).

To understand whether preferential binding of CSN^{CSN7A} to CRL3 or CSN^{CSN7B} to CRL4A has anything to do with cell localization, we determined cellular distribution of the components in cytoplasm, nucleoplasm, and chromatin. However, as shown in Figure S1C, both CSN variants as well as CULs 1, 3, and 4 were mostly equally distributed in HeLa as well as LiSa-2 cells showing low expression in the nucleoplasm of LiSa-2 cells.

In conclusion, immunoprecipitations or pull-downs using single-detergent buffer precipitated latent CSN-CSN^{CSN7A}/CSN^{CSN7B}-CRL1, CSN^{CSN7A}-CRL3, or CSN^{CSN7B}-CRL4A/B complexes occurring in the cytoplasm as well as in the nucleus. In the following, we will focus on latent CSN^{CSN7A}-CRL3 or CSN^{CSN7B}-CRL4A complexes.

CSN^{CSN7A} and CSN^{CSN7B} variant-specific interactomes

In addition to binding CRLs, the CSN has been shown to interact with a variety of other proteins. It binds to the DUBs USP15,[24] USP48,[25] and CYLD.[26] Moreover, the cell cycle inhibitor p27 interacts with the CSN,[16] and regulators of adipogenesis, such as RAB18 and CAV1, were identified as CSN interactors.[17] From the considerable number of CSN-interacting proteins, we selected USP15, p27, RAB18, and CAV1 and asked whether these proteins preferentially bind to CSN^{CSN7A} or CSN^{CSN7B} variants.

As shown in Figure 1E, in undifferentiated LiSa-2 cells, immunoprecipitations of CSN7A co-precipitated almost exclusively USP15 as well as most of RAB18 and CAV1, whereas anti-CSN7B antibody predominantly co-precipitated p27, vanishing traces of USP15 and small amounts of RAB18 and CAV1. Immunoprecipitation of USP15 in HeLa cells led to a co-precipitation of CSN7A (Figure S1D, the band in CSN7B is the antibody light chain), whereas immunoprecipitation of USP48 caused a clear co-precipitation of CSN7B (Figure S1D). RAB18 and CAV1 co-precipitated with CSN7A or CSN7B, whereas p27 and p21 co-precipitated with CSN7B (Figure S1D). Quantification of immunoprecipitations in LiSa-2 cells (Figure 1F) revealed that nearly 100% of USP15 was associated with CSN7A and approximately 75% of p27 bound to CSN7B. RAB18 and CAV1 were mostly found in CSN7A but also in CSN7B precipitations. Whereas CSN5i-3 had no significant impact on protein-protein interactions, MLN4924 reduced binding of all proteins in CSN7B immunoprecipitations (Figure 1F).

Since our results did not yet answer the question of whether the interactors bind to CSN^{CSN7A} or CSN^{CSN7B} or to latent CSN^{CSN7A}-CRL3 and CSN^{CSN7B}-CRL4A complexes, additional experiments were performed.

CSN7A and CSN7B C-terminal 201-stop amino acids are crucial for CRL binding

CSN7A and CSN7B paralogs are characterized by three major amino acid regions: the homologous PCI domain (amino acids 88–177), the unique N-terminal 1–32 amino acids, and C-terminal 201-stop amino acid regions (Figure 2A). Since N-terminal amino acids are mostly involved in CSN activity,[5] we focused on C termini. To study the impact of C-terminal regions on preferential CRL binding, amino acids 201–275 of CSN7A and 201–273 of CSN7B were cut off. FLAG-CSN7A$^{1\text{-}200}$ and FLAG-CSN7B$^{1\text{-}200}$ were stably transfected into LiSa-2 cells and integrated into endogenous CSN complexes (Figure 2B). Western blots in Figure 2B demonstrate that control FLAG pull-downs were characterized by preferential binding of FLAG-CSN7A to CUL3 and FLAG-CSN7B to CUL4A (Pull-down). In contrast, the pull-downs of both FLAG-CSN7A$^{1\text{-}200}$ and FLAG-CSN7B$^{1\text{-}200}$ revealed the loss of preferential binding. In addition, less cullins

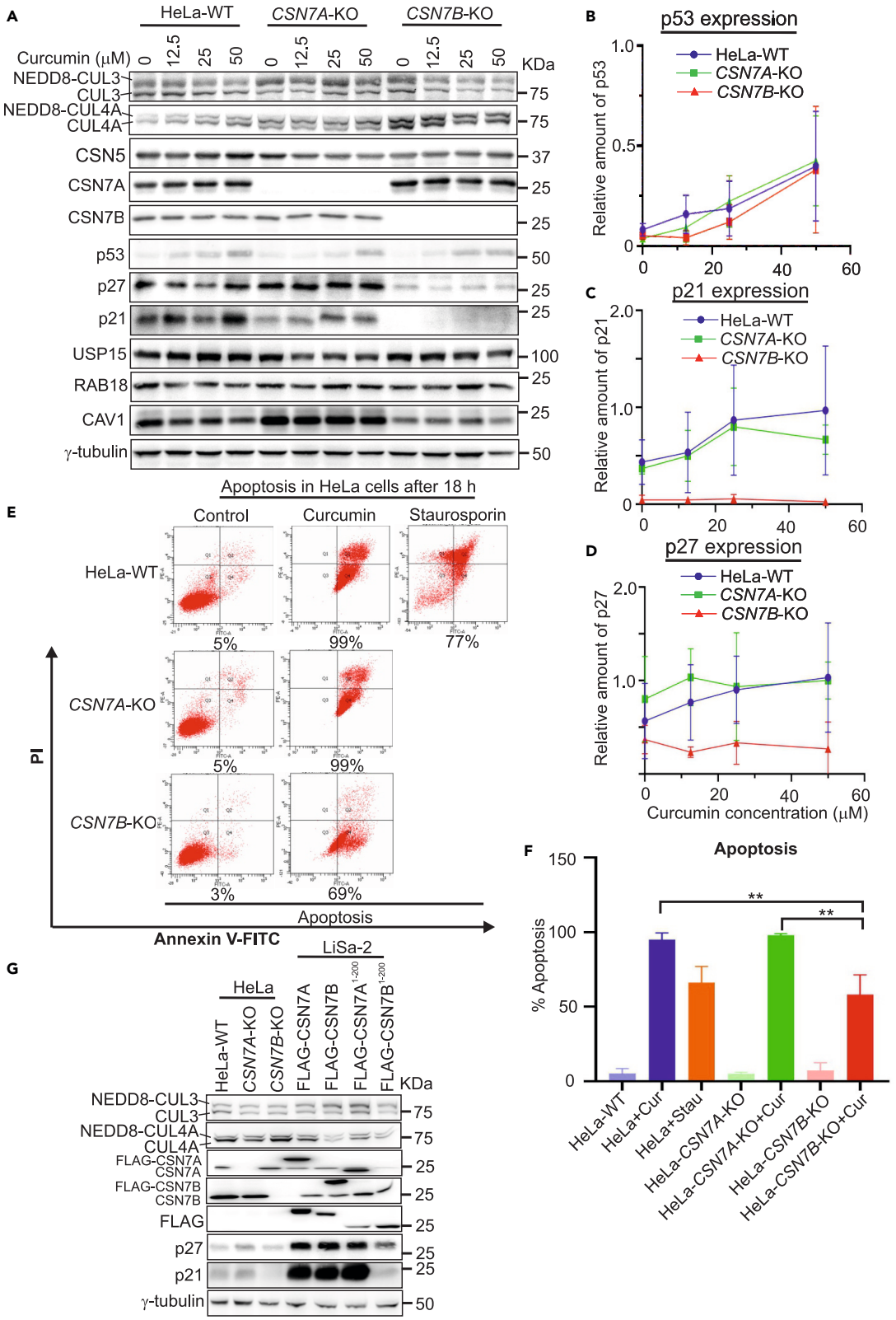
A
HeLa-WT
CSN7A-KO
CSN7B-KO
Curcumin (μM)
0
12.5
25
50
KDa
NEDD8-CUL3
CUL3
NEDD8-CUL4A
CUL4A
CSN5
CSN7A
CSN7B
p53
p27
p21
USP15
RAB18
CAV1
γ-tubulin
75
37
25
50
100
B
p53 expression
Relative amount of p53
C
p21 expression
Relative amount of p21
D
p27 expression
Relative amount of p27
Curcumin concentration (μM)
E
Apoptosis in HeLa cells after 18 h
Control
Curcumin
Staurosporin
HeLa-WT
CSN7A-KO
CSN7B-KO
5%
99%
77%
3%
69%
PI
Annexin V-FITC
Apoptosis
F
Apoptosis
% Apoptosis
HeLa-WT
HeLa+Cur
HeLa+Stau
HeLa-CSN7A-KO
HeLa-CSN7A-KO+Cur
HeLa-CSN7B-KO
HeLa-CSN7B-KO+Cur
G
LiSa-2
HeLa
FLAG-CSN7A
FLAG-CSN7B
FLAG-CSN7A1-200
FLAG-CSN7B1-200
FLAG-CSN7A
FLAG-CSN7B
FLAG

Figure 3. Curcumin-induced apoptotic cell death in HeLa cells requires latent CSN^{CSN7B}-CUL4A complex

(A) HeLa-WT, HeLa-*CSN7A*-KO, and HeLa-*CSN7B*-KO cells were treated with 0, 12.5, 25, and 50 μM of curcumin for 12 h. Lysates were analyzed by indicated antibodies.

(B) Blots in (A) were quantified by densitometry for p53 (n = 3), normalized against γ-tubulin, and means of relative p53 amounts plus/minus SD were plotted against curcumin concentration.

(C) Blots in (A) were quantified by densitometry for p21 (n = 3), normalized against γ-tubulin, and means of relative p21 amounts plus/minus SD were plotted against curcumin concentration.

(D) Blots in (A) were quantified by densitometry for p27 (n = 3), normalized against γ-tubulin, and means of relative p27 amounts plus/minus SD were plotted against curcumin concentration.

(E) HeLa-WT, HeLa-*CSN7A*-KO, and HeLa-*CSN7B*-KO cells were treated with curcumin (50 μM). After 18 h of drug exposure, annexin V staining was analyzed by flow cytometry. Staurosporin (1 μM) was used as reference.

(F) Apoptosis in percent of three independent experiments as shown in (E) (n = 3) was calculated in HeLa-WT, HeLa-WT + curcumin (50 μM) (HeLa-Cur), HeLa-WT + staurosporin (1 μM) (HeLa-Stau), HeLa-*CSN7A*-KO, HeLa-*CSN7A*-KO + curcumin (50 μM) (HeLa-*CSN7A*-KO + Cur), HeLa-*CSN7B*-KO, and HeLa-*CSN7B*-KO + curcumin (50 μM) (HeLa-*CSN7B*-KO + Cur). Data are expressed as % apoptosis. Error bars indicate SDs. Unpaired Student's *t* test was used for statistical analysis. Significant differences are indicated. **p < 0.01.

(G) Lysates of HeLa-WT, HeLa-*CSN7A*-KO, and HeLa-*CSN7B*-KO cells as well as LiSa-2-FLAG-CSN7A, LiSa-2-FLAG-CSN7B, LiSa-2-FLAG-CSN7A$^{1-200}$, and LiSa-2-FLAG-CSN7B$^{1-200}$ were immunoblotted and analyzed with indicated antibodies. Blots are representative of three independent experiments.

1, 3, and 4 were bound to FLAG-CSN7A$^{1-200}$ as well as FLAG-CSN7B$^{1-200}$ complexes as compared to wild-type (WT).

To investigate bindings of USP15 to CSN7A paralog, protein-protein interactions were studied in HeLa cells by co-transfections. HA-USP15 together with FLAG-CSN5, FLAG-CSN7A, or FLAG-CSN7A$^{1-200}$ was co-transfected (Figure 2C, Input). After 16 h, before overexpressed CSN subunits were integrated into endogenous CSN complexes, immunoprecipitations with anti-HA antibody revealed binding of HA-USP15 to FLAG-CSN7A as well as to FLAG-CSN7A$^{1-200}$ but not to FLAG-CSN5 indicating a binding site outside the 201-275 C-terminal amino acid region. Interactions of p27, RAB18, and CAV1 to CSN subunits were analyzed by an *in vitro* translation assay with FLAG-tagged human CSN subunits. Association of glutathione S-transferase (GST)-p27, GST-RAB18, and GST-CAV1 with FLAG-CSN subunits was studied (Figure S1E). In this assay, each FLAG-tagged CSN subunit was *in vitro* translated, mixed with recombinant GST-tagged proteins, and analyzed by immunoblotting.[27] Data in Figure S1E show a direct binding of GST-RAB18 to FLAG-CSN5 and to a lesser extend to FLAG-CSN4. Under these conditions, unmodified GST-p27 and GST-CAV1 did not bind to any recombinant FLAG-CSN subunit. Results were verified by co-transfections in HeLa cells. In Figure 2D, FLAG-CSN7B and EGFP-RAB18 or FLAG-CSN5 and EGFP-RAB18 as well as FLAG-CSN7B and FLAG-p27 or FLAG-CSN5 and FLAG-p27 were co-transfected (Input). After 16 h, immunoprecipitations with anti-RAB18 or anti-p27 antibodies confirmed binding of EGFP-RAB18 to FLAG-CSN5 and approved binding of FLAG-p27 to FLAG-CSN5 (Figure 2D, IP: RAB18 and IP: p27).[28]

Curcumin-induced apoptotic cell death in HeLa cells needs latent CSN^{CSN7B}-CRL4A complexes

We used curcumin, a natural polyphenolic compound derived from the plant *Curcuma longa*, to induce apoptosis. Curcumin blocks the activity of kinases including CSN-associated kinases such as CK2, Akt, and PKD resulting in accumulation of p53, p27, and p21.[29,30] We applied HeLa WT cells and *CSN7A* or *CSN7B* HeLa KOs to analyze the mutual dependence among CSN, CSN-associated proteins, and curcumin-dependent apoptosis. For this purpose, we used CRISPR/Cas9 to generate *COPS7A/CSN7A* or *COPS7B/CSN7B* loss-of-function HeLa cells.[20] HeLa-*CSN7A*-KO and HeLa-*CSN7B*-KO cells completely lost the deleted proteins but retained viability as well as the expression of the respective alternative CSN7 paralog protein (Figure 3A). Stability of selected proteins was estimated by western blotting after addition of 0, 12.5, 25, and 50 μM curcumin. As demonstrated in Figure 3A, incubation for 12 h led to a curcumin concentration-dependent stabilization of p53 in HeLa-WT as well as in *CSN7A* and *CSN7B* KO cells (Figure 3B). Curcumin did not affect CUL3 or CUL4A neddylation/deneddylation, CSN5, CSN7A or CSN7B, and USP15 or RAB18. Interestingly, CAV1 expression was considerably elevated in *CSN7A*-KO cells. In HeLa-WT and *CSN7A*-KO cells, expression of p21 and p27 increased up to 12.5 μM or 25 μM of curcumin, respectively, and reached a plateau at 50 μM, probably by increasing cell death (Figures 3C and 3D). In contrast, in HeLa-*CSN7B*-KO cells, p21 was almost zero and p27 remained on a low level independent of p53 increase (Figures 3A–3D). Inhibitors of neddylation/deneddylation, MLN4924, and CSN5i-3, as well as of the ubiquitin proteasome system (UPS), MG132, were preincubated for 2 h and subsequently

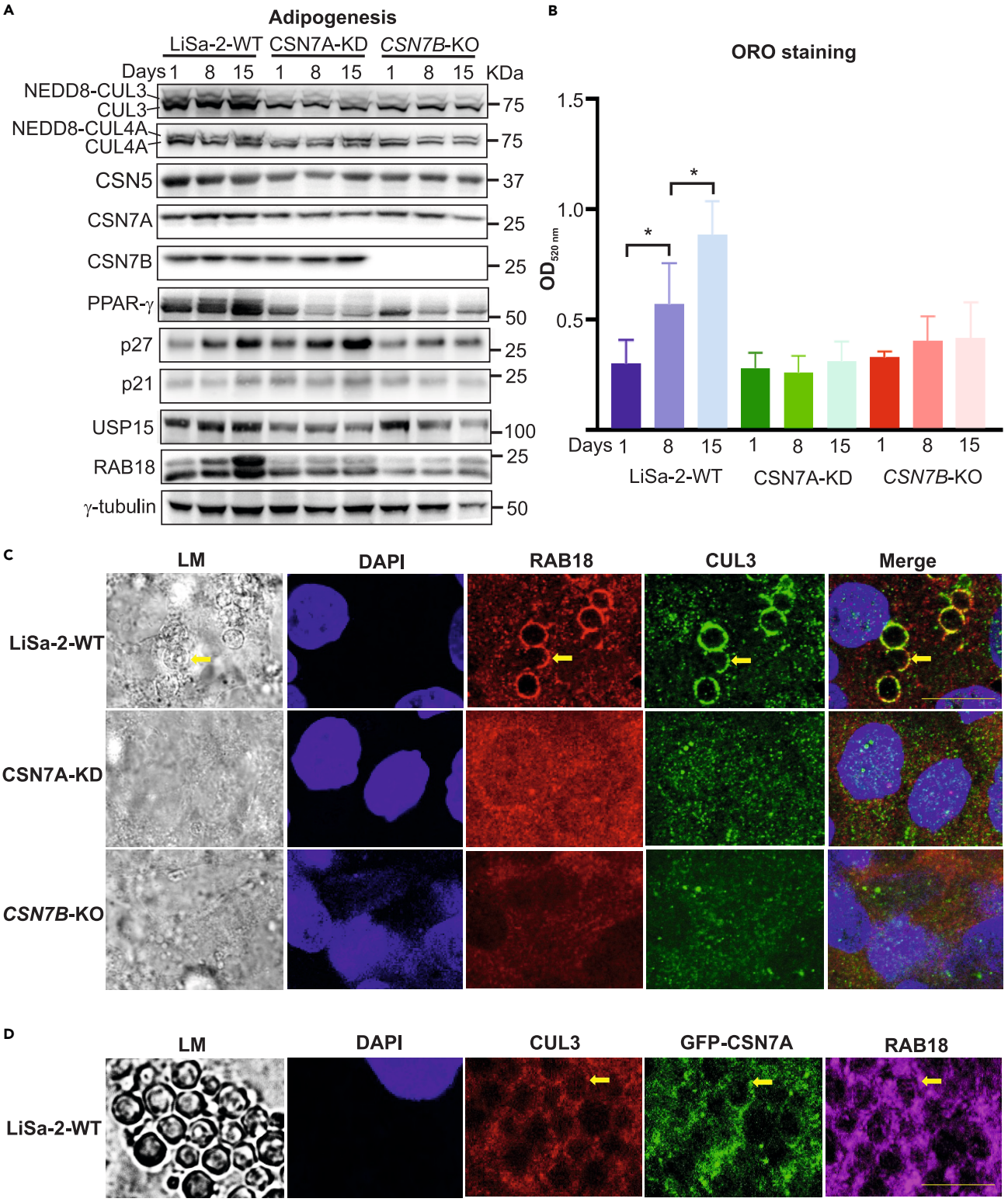

Figure 4. RAB18 recruits CSN^{CSN7A}-CRL3 complexes to LD membranes during adipogenesis in LiSa-2 cells

(A) LiSa-2-WT, LiSa-2-CSN7A-KD, and LiSa-2-*CSN7B*-KO cell lysates were analyzed with indicated antibodies after 1, 8, and 15 days of adipogenic differentiation.

Figure 4. *Continued*

(B) LiSa-2-WT, LiSa-2-CSN7A-KD, and LiSa-2-*CSN7B*-KO cells were stained with ORO and quantified by photometry. Data obtained from three different experiments are expressed as means of relative amounts plus/minus SD. Student's t-test was used for statistical analysis. *$p < 0.1$.

(C) LiSa-2-WT, LiSa-2-CSN7A-KD, and LiSa-2-*CSN7B*-KO cells were analyzed by light microscopy (LM) and confocal fluorescence microscopy. After 15 days of adipogenic differentiation, cells were stained with specific antibodies as indicated and analyzed by confocal microscopy. Cell nuclei were stained with DAPI. Regions of interest such as LDs are shown with yellow arrow. The yellow bar in Merge channel corresponds to 15 μm.

(D) LiSa-2-WT cells were stably transfected with GFP-CSN7A. After 15 days of adipogenic differentiation, CUL3 and RAB18 were stained with specific primary antibodies as indicated and with species-appropriate fluorescence secondary antibodies, Alexa Flour 647 (red) and Cy3 (magenta), respectively, and analyzed by confocal microscopy. Cell nuclei were stained with DAPI. Regions of interest such as LDs are shown with yellow arrow. The yellow bar channel corresponds to 15 μm.

treated with 50 μM curcumin for 10 h. Under these conditions, p27 in HeLa-*CSN7B*-KO cells was mostly stabilized indicating degradation by the UPS (Figure S1F). Since CSN^{CSN7B} preferentially binds to CUL4A (Figure 1C), a component of CRL4A, we concluded that *CSN7B* KO led to release of CRL4A from latent CSN^{CSN7B}-CRL4A complexes and, consequently, to uncontrolled $_{NEDD8}CRL4A^{CDT2}$-dependent ubiquitylation and subsequent degradation of p21 and p27.[31,32]

Apoptosis was determined by flow cytometry analysis after 18 h of treatment with 50 μM curcumin (Figure 3E). Staurosporin (1 μM)-induced apoptosis was used as control. In untreated HeLa-WT, HeLa-*CSN7A*-KO, and HeLa-*CSN7B*-KO cells, the apoptotic fraction was low (3–5%). Upon treatment with curcumin, HeLa-WT and HeLa-*CSN7A*-KO cells were characterized by apoptosis of almost 100%. In contrast, apoptosis in HeLa-*CSN7B*-KO cells was only 69%. We concluded that *CSN7B* KO cells were partially resistant against curcumin in contrast to WT and *CSN7A*-KO cells. To deepen the data, three independent experiments were calculated (Figure 3F). While curcumin-induced apoptosis in HeLa-WT and in HeLa-*CSN7A*-KO cells was almost 100%, significant reduction of cell death was measured in HeLa-*CSN7B*-KO.

Based on our observation that apoptotic cell death needs stabilization of p21 and p27 which only occurred in presence of the latent CSN^{CSN7B}-CRL4A complex, we used stably transfected LiSa-2-FLAG-$CSN7A^{1-200}$ and LiSa-2-FLAG-$CSN7B^{1-200}$ knowing that the C termini are necessary for latent CSN-CRL complex stability. As demonstrated in Figure 3G, p21 and p27 were reduced in HeLa-*CSN7B*-KO cells as compared to HeLa-WT and HeLa-*CSN7A*-KO cells. Likewise, in LiSa-2-FLAG-CSN7A, LiSa-2-FLAG-CSN7B, and LiSa-2-FLAG-$CSN7A^{1-200}$, expressions of p21 and p27 were high. On the contrary, in LiSa-2-FLAG-$CSN7B^{1-200}$ cells, steady-state levels of p21 and p27 were significantly reduced. This confirms our hypothesis that p21/p27 stabilization in G1 phase and apoptosis can only be accomplished in presence of latent CSN^{CSN7B}-CRL4A complex. This was confirmed by the fact that reduced apoptotic cell death in HeLa-*CSN7B*-KO cells can be rescued by overexpression of FLAG-CSN7B but not of FLAG-$CSN7B^{1-200}$. In HeLa-*CSN7A*-KO and HeLa-*CSN7B*-KO, apoptosis was induced by 50 μM curcumin for 12 h (Figure S2A). Under this condition, apoptosis in HeLa-*CSN7B*-KO cells was reduced below 40% compared to HeLa-*CSN7A*-KO cells. Overexpression of FLAG-CSN7B in HeLa-*CSN7B*-KO cells rescued apoptosis to more than 60%, whereas overexpression of FLAG-$CSN7B^{1-200}$ was without effect.

RAB18 recruits latent CSN^{CSN7A}-CRL3 complex to lipid droplets during adipogenesis

We asked whether interactors of the CSN influence adipogenesis in LiSa-2 preadipocytes. To this end, we applied LiSa-2-WT, LiSa-2-CSN7A-knockdown (KD), and LiSa-2-*CSN7B*-KO cells and induced adipogenesis by culturing cells in serum-free medium with supplements including 1 nM insulin, 20 p.m. triiodothyronine, and 1 mM cortisol according to an earlier protocol.[33] LiSa-2-CSN7A-KD cells were used because KO of *CSN7A* in LiSa-2 cells is lethal in contrast to HeLa and AD293 cells.[20] In Figure 4A, CSN7A-KD led to a reduction of CSN7A protein by about 50% compared to LiSa-2-WT, whereas *CSN7B*-KO caused a complete deletion of CSN7B protein. In LiSa-2-WT, the typical increase of neddylated CUL3 during 1, 8, and 15 days of adipogenesis was detected,[17] but not in CSN7A KD or in *CSN7B* KO cells. In parallel, a time-dependent elevation of the peroxisome proliferator-activated receptor-γ (PPAR-γ), the master regulator of adipogenesis,[34] was detected in LiSa-2-WT (Figure 4A). On the contrary, PPAR-γ expression was reduced after 8 and 15 days in CSN7A-KD and in *CSN7B*-KO cells. On the other hand, p27 expression increased in LiSa-2-WT and LiSa-2-CSN7A-KD but not in LiSa-2-*CSN7B*-KO cells, whereas p21 and USP15 mostly remained unchanged.

Especially RAB18 attracted our interest. Physical interaction between RAB18 and CUL3 on LD membranes and adipogenesis-dependent accumulation of RAB18 and of neddylated CUL3 in LiSa-2-WT cells were

shown.[17] Moreover, in contrast to HeLa cells and undifferentiated LiSa-2 cells in which RAB18 occurs as a single band, in differentiating LiSa-2 cells, the protein was identified as a double band: a fast-migrating form and a slower-migrating most likely phosphorylated RAB18 (Figure 4A) as described for other RAB proteins as well.[35] Indeed, LiSa-2-WT cells were characterized by a significant accumulation of the RAB18 doublet during 8 and 15 days of adipogenesis. In LiSa-2-CSN7A-KD and LiSa-2-*CSN7B*-KO cells, the typical adipogenic increase of RAB18 did not take place and neddylated CUL3 did not accumulate (Figure 4A). Oil Red O (ORO) staining of LiSa-2-WT in Figure S2B confirmed an increase of lipids accumulating in LDs during adipogenesis. On the other hand, neither CSN7A-KD nor *CSN7B*-KO cells showed significant lipid production (Figure S2B). Quantification of ORO staining based on three independent experiments revealed a clear proportional increase of lipid accumulation in LiSa-2-WT during adipogenesis. In contrast, both CSN7A-KD and *CSN7B*-KO cells had no lipid accumulation (Figure 4B).

To study co-localization of RAB18, CSN, and CUL3 in LiSa-2-WT, LiSa-2-CSN7A-KD, and in LiSa-2-*CSN7B*-KO cells, we performed confocal fluorescence microscopy after 15 days of differentiation (Figure 4C). In LiSa-2-WT, LDs were formed during adipogenesis as demonstrated in light microscopy (LM) and in confocal fluorescence microscopy. Merge confirmed a co-localization of RAB18 and CUL3 on the membrane surface of LDs. On the contrary, CSN7A-KD and *CSN7B*-KO cells did not exhibit detectable LDs indicating the need of both CSN7A and CSN7B for LD biogenesis. Moreover, after 15 days of adipogenesis, confocal fluorescence microscopy showed binding of CSN^{CSN7A} but not of CSN^{CSN7B} to LD membrane together with CUL3 (Figure S2C). Thus, in LiSa-2-WT, RAB18, CSN^{CSN7A}, and CUL3 co-localized to the LD outer membrane. In contrast, in CSN7A-KD and *CSN7B*-KO, RAB18 and CUL3 diffusely spread in cells and LDs were not detectable after 15 days of adipogenesis. To demonstrate the simultaneous binding of CUL3, CSN7A, and RAB18 to LDs after 15 days of adipogenesis, CUL3 and RAB18 were stained with specific primary antibodies as indicated and with species-appropriate fluorescence secondary antibodies Alexa Flour 647 (red) and Cy3 (magenta), respectively. In addition, GFP-CSN7A (green) was integrated into endogenous CSN[20] and served as third color for staining (Figure 4D). Images demonstrate simultaneous binding to LD membranes of the three components, CUL3, GFP-CSN7A, and RAB18.

To make sure that RAB18 binds to CSN7A as well as to CUL3, immunoprecipitations were performed. As demonstrated in Figure S2D, during adipogenesis the RAB18 doublet increased and captured more and more CSN7A and CUL3 proteins most likely as latent CSN^{CSN7A}-CRL3 complex.

We postulated that RAB18, perhaps phosphorylated RAB18, recruits the latent CSN^{CSN7A}-CRL3 complex to LDs, where it is gradually activated/neddylated. Binding of RAB18 to CSN5 (Figures S1E and 2D) might block deneddylation. Therefore, downregulation of RAB18 should produce a similar phenotype as obtained with silencing of CSN7A. After 8 days of adipogenesis, RAB18 protein was reduced by 80% using specific siRAB18, which caused a significant reduction of CUL3 neddylation by about 50% (Figures 5A and 5B). In contrast, calculation of CUL4A neddylation/deneddylation ration did not show any change with or without RAB18 (Figure 5C). In addition, treatment with siRAB18 induced a clear diminution of ORO staining and blocked adipogenesis (Figures 5D and 5E).

Since the stability of the latent CSN^{CSN7A}-CRL3 complex is assured by the C terminus of CSN7A and that of CSN^{CSN7B}-CRL4A, by the C terminus of CSN7B, we used stably transfected LiSa-2-FLAG-$CSN7A^{1-200}$ and LiSa-2-FLAG-$CSN7B^{1-200}$ cells with integrated FLAG-$CSN7A^{1-200}$ and FLAG-$CSN7B^{1-200}$ to study their impact on adipogenesis. While expression of selected proteins in LiSa-2-FLAG-CSN7A and LiSa-2-FLAG-CSN7B cells did not much differ from WT cells, significantly different protein levels were obtained in LiSa-2-FLAG-$CSN7A^{1-200}$ and LiSa-2-FLAG-$CSN7B^{1-200}$ cells (Figure S3A). Cutting off the C termini caused a reduction of neddylated CUL3, p27, and RAB18 expression. In addition, both CSN7A and CSN7B truncations led to a clear retardation of adipogenesis compared to LiSa-2-WT and LiSa-2-FLAG-CSN7A as well as LiSa-2-FLAG-CSN7B cells as indicated by ORO staining (Figure S3B). We concluded that adipogenesis needs both the latent CSN^{CSN7A}-CRL3 complex, which is recruited by RAB18 and activated at LD membranes, and the latent CSN^{CSN7B}-CRL4A complex, necessary for p27 accumulation, a hallmark for adipogenesis.[36]

DISCUSSION

Here we demonstrate that the CSN variants, CSN^{CSN7A} and CSN^{CSN7B}, are firmly coupled to CRLs and form latent CSN-CRL complexes, which represent a quick reservoir for diverse cellular functions. Additional

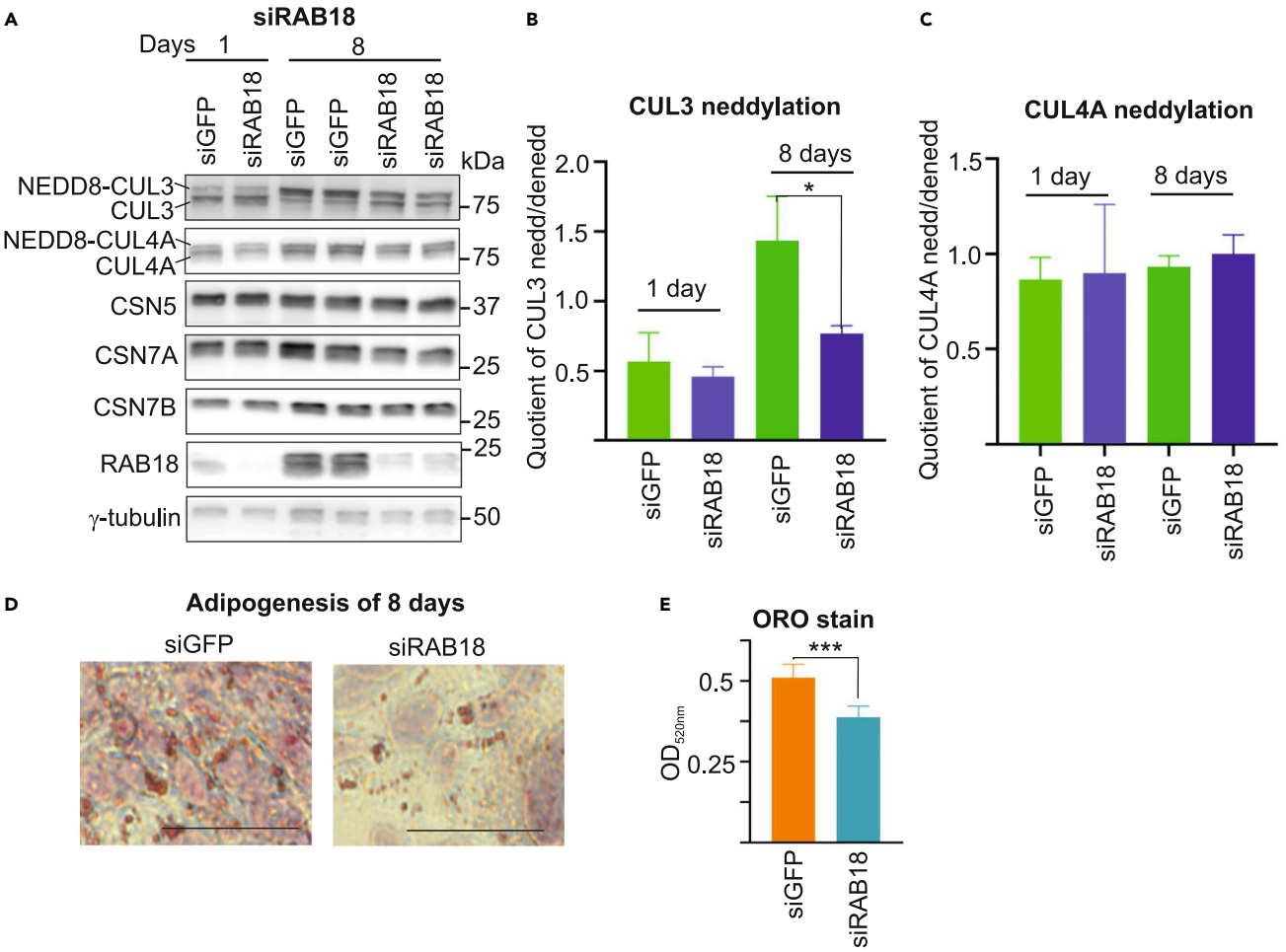

Figure 5. Recruited CUL3 is neddylated on LD membrane during adipogenesis in LiSa-2 cells

(A) Control siRNA (siGFP) and specific siRNA against RAB18 (siRAB18) were transfected into LiSa-2 cells. After 48 h transfected cells were incubated for 1 and 8 days of adipogenesis. After 8 days samples are presented as doublet: 2 x siGFP and 2 x siRAB18.

(B) Blots in (A) were quantified by densitometry for neddylated and deneddylated CUL3 (n = 4), normalized against γ-tubulin and expressed as means of relative amounts of neddylated CUL3 divided by deneddylated CUL3 plus/minus SD. Unpaired Student's t-test was used for statistical analysis. *$p < 0.05$.

(C) Blots in (A) were quantified by densitometry for neddylated and deneddylated CUL4A (n = 4), normalized against γ-tubulin and expressed as means of relative amounts of neddylated CUL4A divided by deneddylated CUL4A plus/minus SD.

(D) LiSa-2 cells were preincubated with control (siGFP) and with siRAB18 for 48 h. After 8 days of adipogenesis control cells (siGFP) and siRAB18 cells were stained with ORO and analyzed with light microscopy. Bars represent 50 μm.

(E) Stains shown in (D) were quantified by photometry measuring ORO with OD_{520nm}. Data obtained from three different experiments are expressed as means of relative amounts plus/minus SD. Student's t-test was used for statistical analysis. ***$p < 0.1$.

ligands such as USP15, p27, RAB18, or CAV1 are associated with latent CSN-CRL complexes supporting their actions. Disintegration of the latent CSN-CRL complexes lead to disruption of normal cell operations.

Interestingly, USP15 specifically interacts with CSN7A forming a multi-DUB complex with the CSN^{CSN7A} variant. It precipitates together with the latent CSN^{CSN7A}-CRL3. USP15 and perhaps CYLD in liver cells[26] most likely protect CRL3 from autoubiquitylation. However, currently the exact function of USP15 in CSN^{CSN7A}-CRL3 complexes is not known. Although CAV1 precipitates with CSN7A and CSN7B and was detected on LDs,[17,37] *in vitro*, it does not bind to any CSN subunit (Figure S1E). Whether CAV1 is associated via CUL3[17] or needs additional modifications or other proteins for binding to CSN-CRL complexes will be elucidated in future experiments. In Table S1 most protein-protein interactions in HeLa and in undifferentiated LiSa-2 cells described in this paper are summarized. In the following, we will focus on mechanisms of CSN^{CSN7A} and CSN^{CSN7B} variants binding to CRL3 or CRL4A/B, respectively, as well as to actions of p27 in curcumin-induced apoptosis and the specific role of RAB18 in adipogenesis.

Although CSN-mediated deneddylation is redundant,[20] we found preferential binding of CSN^{CSN7A} to CRL3 and CSN^{CSN7B} to CRL4A/B. Under used conditions, preferential association of CSN variants with CRL3 or CRL4A/B is independent of CRL neddylation/deneddylation, as indicated by CSN5i-3 and MLN4924 inhibitors (Figures 1D and S1A). Most importantly, preferential binding of CSN^{CSN7A} to CRL3 is determined by the C-terminal 201–275 amino acids of CSN7A, and that of CSN^{CSN7B} to CRL4, by the C-terminal 201–273 amino acids of CSN7B (Figure 2B). In other words, the unique C-terminal 201 - stop amino acids of CSN7A and CSN7B prefer either CRL3 or CRL4, respectively.

One reason for the preferential binding might be the distribution of CSN variants and CRLs in cells. However, cellular spreading of these complexes determined by standard methods did not substantially differ (Figure S1C). More likely and as discussed below, preferential binding is another level of regulation in which latent CSN^{CSN7A}-CRL3 and CSN^{CSN7B}-CRL4A/B complexes serve as reservoirs for specific cellular functions.

Apoptosis induced by curcumin upregulates p53, even in low p53-expressing HeLa cells, causing G1 cell-cycle arrest via p21 and p27 accumulation leading to apoptosis.[29,30] Originally, p27 binding to CSN5[16] as a consequence of phosphorylation at its C terminus[28] has been described, which was confirmed in our experiments (Figure 2D). Interestingly, our immunoprecipitations in LiSa-2 cells revealed almost exclusive precipitation of p27 with CSN7B and vice versa (Figures 1E and S1D), indicating a dominant binding of p27 to latent CSN^{CSN7B}-CRL4A complexes. Latent CSN^{CSN7B}-CRL4A complex has a specific binding site for p27, CDT2, the SR of CRL4A. It is known that $CRL4A^{CDT2}$ regulates G1 cell cycle progression and its primary target in G1 phase is the cyclin-dependent kinase (CDK) inhibitor p27.[31,32] Under normal cell conditions, low steady-state p27 levels are adjusted by low free $_{NEDD8}CRL4A^{CDT2}$. Curcumin induces increase of p27 in HeLa-WT and in HeLa-*CSN7A*-KO cells leading to cell-cycle arrest in G1 and allowing development of apoptosis (Figures 3E and 3F). In contrast, the KO of *CSN7B* causes release of substantial amounts of free CRL4A, which in activated and undamped form, $_{NEDD8}CRL4A^{CDT2}$, quickly ubiquitylates p21 and p27 for degradation preventing G1 arrest and apoptosis. By cutting off the 201-273 C-terminal amino acids of CSN7B, which also leads to disintegration of CSN^{CSN7B}-CRL4A complexes, our hypothesis was proven. Expression of p21 as well as of p27 was drastically reduced (Figure 3G). Consistently, apoptosis in *CSN7B* KO cells was rescued by full-length FLAG-CSN7B but not by the truncated FLAG-$CSN7B^{1-200}$ version (Figure S2A).

RAB18 is an essential component of LDs, and depending on insulin it accumulates on the surface of the organelles.[38] RAB proteins cycle between a guanosine diphosphate (GDP)-bound inactive state, localized in the cytosol, and a membrane-associated guanosine triphosphate (GTP)-bound, active conformation.[39] We hypothesize that the active and phosphorylated form of RAB18 recruits latent CSN^{CSN7A}-CRL3 complex to LD membranes by direct binding to CUL3 (Figure S2D). At the LD membrane CRL3 is activated by neddylation (Figure 5B). Additional binding of RAB18 to CSN5 might suppress CRL3 deneddylation. Activated CRL3 ubiquitylates proteins like C/EBP-homologous protein (CHOP),[12] ras homolog gene family, member A (RHOA),[17] and other not yet identified substrates important for LD formation and adipogenesis. What is the evidence of this hypothesis? (i) In LiSa-2-WT cells, RAB18 binds to CSN4/CSN5 (Figures 2D and S1E) as well as to CUL3 (Figure S2D). (ii) During adipogenesis, RAB18, CUL3 (Figure 4C), and CSN^{CSN7A} (Figure S2C) co-localize to LD membranes (Figures 4C and 4D). (iii) Downregulation of RAB18 reduces CUL3 neddylation (Figure 5B), prevents formation of LDs, and blocks adipogenesis (Figures 5D and 5E). (iv) Cutting off the 201-275 C-terminal amino acids of CSN7A retards adipogenesis in LiSa-2 cells (Figure S3).

Interestingly, just recently, another CRL3 "activation" at the endoplasmic reticulum by releasing the SR KLHL12 from the membrane and fixing it at CUL3 was shown.[40] It would be interesting to see at which stage CSN^{CSN7A} is associated with the $CRL3^{KLHL12}$ complex. Remarkably, the interaction between CSN-CRL can be modified by the metabolite inositol hexaphosphate (IP6). IP6-assisted CSN-COP1 competition regulates CRL4 activity controlling glucose-induced insulin secretion[41] indicating that IP6 is an important regulator of latent CSN-CRL complex formation.

In our hands, CSN variants are essential for adipogenesis. KD of CSN7A causes significant reduction of CSN^{CSN7A} variant releasing free CRL3 from latent complexes which, however, cannot be recruited by RAB18 to LD membranes. Therefore, LD biogenesis and adipogenesis are blocked. In case of *CSN7B* KO, we face a similar situation as with apoptosis. Absence of the CSN^{CSN7B} complex releases uninhibited

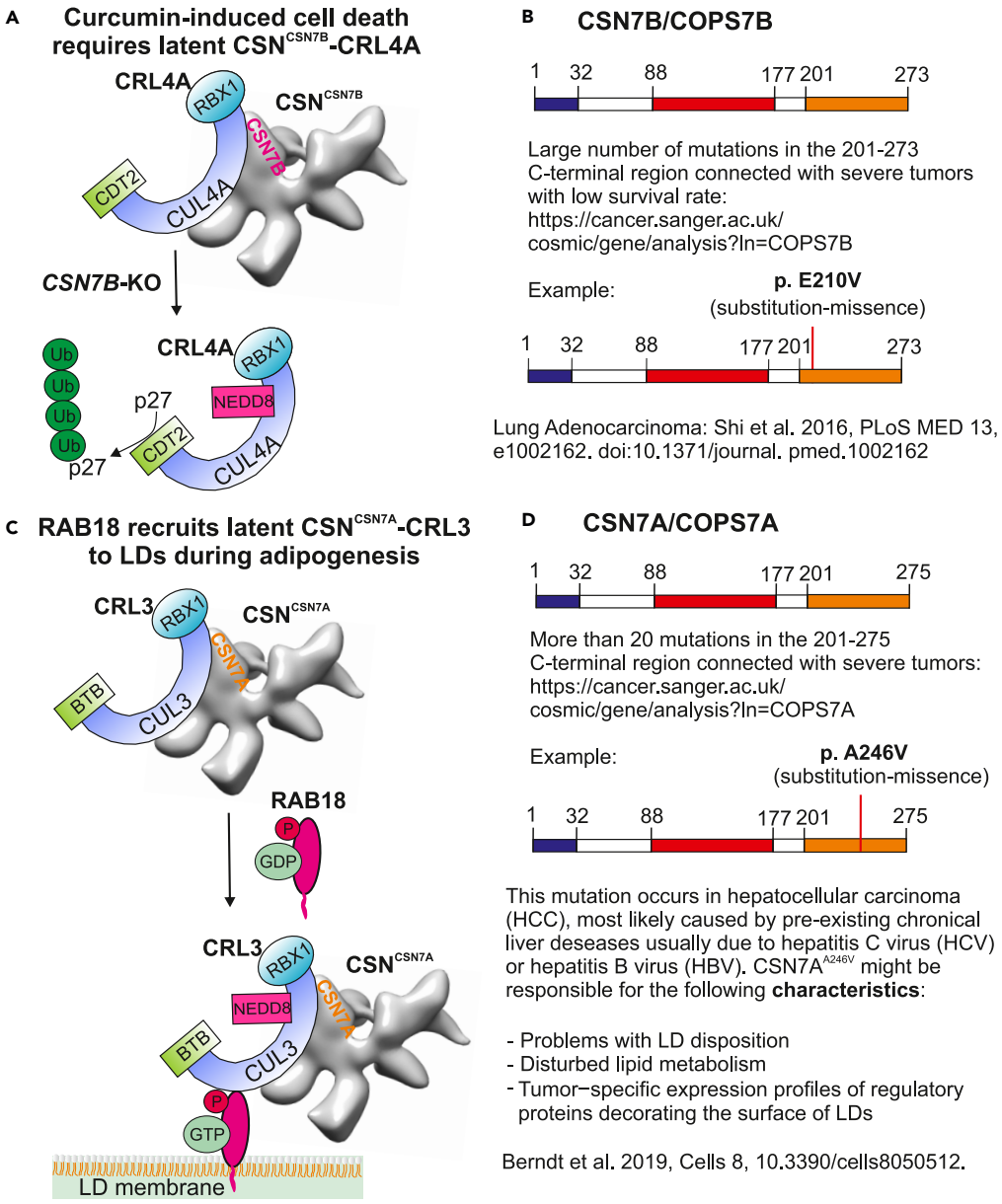

Figure 6. Models of curcumin-induced cell death in HeLa cells and LD formation during adipogenesis in LiSa-2 cells

(A) Curcumin blocks the activity of serine-threonine kinase Akt and nuclear factor kappa of activated B cells (NF-κB) signaling which leads to increase of p53, p21, p27, and caspase signaling. The presence of latent CSN^{CSN7B}-CRL4A complex prevents ubiquitylation and degradation of p21 and p27. The consequence is an arrest of cell cycle and apoptosis. As a result of *CSN7B* knockout, the CRL4A activity lost its natural brake, the CSN^{CSN7B} variant, which causes rapid ubiquitylation/degradation of p21 and p27. Therefore, HeLa-*CSN7B*-KO cells have no cell-cycle arrest and reduced apoptosis. They are characterized by high resistance against curcumin-induced apoptosis.

(B) Mutations in the 201–273 amino acids region of CSN7B were obtained from https://cancer.sanger.ac.uk/. For instance, mutation of Glu210 to Val (E210V) causing a missense substitution in the CSN7B C terminus is published in Shi et al.[43]

(C) As a prerequisite of LD formation, RAB18, presumably in its phosphorylated GTP-RAB18 form, recruits CSN^{CSN7A}-CRL3 to LD membranes. At the outer LD membrane CSN^{CSN7A}-CRL3 is activated by neddylation, whereas CSN^{CSN7A} deneddylation is probably inhibited by RAB18 binding to CSN5. In case of CSN7A knockdown, not enough CSN^{CSN7A}-CRL3 complex can be recruited to LDs by RAB18. Under this condition, LD formation is blocked. Likewise, cutting off the

Figure 6. *Continued*
C-terminal ends of CSN7A, which results in disintegration of the latent CSN^{CSN7A}-CRL3 complex, also leads to a blockade of LD formation and of adipogenesis.
(D) Mutations in the C-terminal 201–275 amino acid region of CSN7A were obtained from https://cancer.sanger.ac.uk/. An example is the substitution of Ala246 by Val (A246V) published in Berndt et al.[42]

$_{NEDD8}CRL4A^{CDT2}$ causing degradation of p21/p27 and preventing G1 cell-cycle arrest. Under these conditions adipogenesis is inhibited since increase of p27 is a prerequisite and hallmark of adipogenesis.[36]

Consistent with the described scenarios is our observation that tumors with mutations in the CSN7A or CSN7B C termini are characterized by problems of LD disposition and apoptosis, respectively (Figures 6B and 6D). Data from https://cancer.sanger.ac.uk/revealed tumors characterized by mutations in the 201-stop amino acid regions of CSN7A or CSN7B paralogs. However, the mechanism behind how CSN-CRL axis interplays between carcinogenesis and lipid droplets remains unclear, and further experimental validation will be necessary.

In conclusion, our data provide new insights into the functions of CSN^{CSN7A} and CSN^{CSN7B} variants operating in latent CSN^{CSN7A}-CRL3 and latent CSN^{CSN7B}-CRL4A complexes which represent basic prerequisites of adipogenesis and apoptosis. Disruption of the latent CSN-CRL complexes gives rise to diseases including obesity and tumor.

Limitations of the study

We must acknowledge that, so far, there exists no knowledge on lipid droplet dysfunctions and carcinogenesis and any role of CSN-CRL complexes in the process. We are just at the beginning to understand how lipid droplets are formed. Further experimental efforts will be necessary to establish the direct causal link.

STAR★METHODS

Detailed methods are provided in the online version of this paper and include the following:

- KEY RESOURCES TABLE
- RESOURCE AVAILABILITY
  - Lead contact
  - Materials availability
  - Data and code availability
- EXPERIMENTAL MODEL
- METHOD DETAILS
  - Plasmid transfections and stable cell lines
  - RNA interference
  - Protein extraction, immunoblotting and immunoprecipitation
  - FLAG pulldowns
  - Subcellular fractionation
  - *In vitro* and cell binding assays
  - Curcumin-induced apoptosis and monitoring by flow cytometry analysis
  - Adipogenesis and ORO staining
  - Immunostaining and confocal fluorescence microscopy
- QUANTIFICATION AND STATISTICAL ANALYSIS

SUPPLEMENTAL INFORMATION

Supplemental information can be found online at https://doi.org/10.1016/j.isci.2023.106468.

ACKNOWLEDGMENTS

This work was funded in part by grant 31770813 awarded by the Natural Science Foundation of China to W.D., by the European Union Program European Regional Development Fund of the Ministry of Economy, Science and Digitalisation in Saxony Anhalt within the Center of Dynamic Systems (ZS/2016/04/78155) to W.D. and M.N., and by the German Research Foundation from RTG 2408 (361210922) to M.N.

AUTHOR CONTRIBUTIONS

Conceptualization, W.D. and D.D.; Methodology, D.D., R.H., J.W., and S.C.; Formal Analysis, D.D., R.H., J.W., and W.D.; Investigation, D.D., R.H., J.W., and S.C.; Writing – Original Draft, W.D. and D.D.; Writing – Review & Editing, W.D., D.D., and M.N.; Visualization, D.D. and R.H.; Supervision, D.D., W.D., and M.N.; Funding Acquisition, W.D. and M.N.

DECLARATION OF INTERESTS

The authors declare no competing interests.

INCLUSION AND DIVERSITY

We support inclusive, diverse, and equitable conduct of research.

Received: March 31, 2022
Revised: February 14, 2023
Accepted: March 20, 2023
Published: March 22, 2023

REFERENCES

1. Deng, X.W., Dubiel, W., Wei, N., Hofmann, K., Mundt, K., Colicelli, J., Kato, J., Naumann, M., Segal, D., Seeger, M., et al. (2000). Unified nomenclature for the COP9 signalosome and its subunits: an essential regulator of development. Trends Genet. *16*, 203–289.

2. Hofmann, K., and Bucher, P. (1998). The PCI domain: a common theme in three multiprotein complexes. Trends Biochem. Sci. *23*, 204–205.

3. Lingaraju, G.M., Bunker, R.D., Cavadini, S., Hess, D., Hassiepen, U., Renatus, M., Fischer, E.S., and Thomä, N.H. (2014). Crystal structure of the human COP9 signalosome. Nature *512*, 161–165.

4. Rockel, B., Schmaler, T., Huang, X., and Dubiel, W. (2014). Electron microscopy and in vitro deneddylation reveal similar architectures and biochemistry of isolated human and Flag-mouse COP9 signalosome complexes. Biochem. Biophys. Res. Commun. *450*, 991–997.

5. Cavadini, S., Fischer, E.S., Bunker, R.D., Potenza, A., Lingaraju, G.M., Goldie, K.N., Mohamed, W.I., Faty, M., Petzold, G., Beckwith, R.E.J., et al. (2016). Cullin-RING ubiquitin E3 ligase regulation by the COP9 signalosome. Nature *531*, 598–603. https://doi.org/10.1038/nature17416.

6. Cope, G.A., and Deshaies, R.J. (2003). COP9 signalosome: a multifunctional regulator of SCF and other cullin-based ubiquitin ligases. Cell *114*, 663–671.

7. Mosadeghi, R., Reichermeier, K.M., Winkler, M., Schreiber, A., Reitsma, J.M., Zhang, Y., Stengel, F., Cao, J., Kim, M., Sweredoski, M.J., et al. (2016). Structural and kinetic analysis of the COP9-Signalosome activation and the cullin-RING ubiquitin ligase deneddylation cycle. Elife *5*, e12102. https://doi.org/10.7554/eLife.12102.

8. Faull, S.V., Lau, A.M.C., Martens, C., Ahdash, Z., Hansen, K., Yebenes, H., Schmidt, C., Beuron, F., Cronin, N.B., Morris, E.P., and Politis, A. (2019). Structural basis of Cullin 2 RING E3 ligase regulation by the COP9 signalosome. Nat. Commun. *10*, 3814. https://doi.org/10.1038/s41467-019-11772-y.

9. Dubiel, W., Chaithongyot, S., Dubiel, D., and Naumann, M. (2020). The COP9 signalosome: a multi-DUB complex. Biomolecules *10*, 1082. https://doi.org/10.3390/biom10071082.

10. Schmidt, M.W., McQuary, P.R., Wee, S., Hofmann, K., and Wolf, D.A. (2009). F-box-directed CRL complex assembly and regulation by the CSN and CAND1. Mol. Cell *35*, 586–597.

11. Pierce, N.W., Lee, J.E., Liu, X., Sweredoski, M.J., Graham, R.L.J., Larimore, E.A., Rome, M., Zheng, N., Clurman, B.E., Hess, S., et al. (2013). Cand1 promotes assembly of new SCF complexes through dynamic exchange of F box proteins. Cell *153*, 206–215.

12. Dubiel, D., Ordemann, J., Pratschke, J., Dubiel, W., and Naumann, M. (2015). CAND1 exchange factor promotes Keap1 integration into cullin 3-RING ubiquitin ligase during adipogenesis. Int. J. Biochem. Cell Biol. *66*, 95–100. https://doi.org/10.1016/j.biocel.2015.07.013.

13. Reitsma, J.M., Liu, X., Reichermeier, K.M., Moradian, A., Sweredoski, M.J., Hess, S., and Deshaies, R.J. (2017). Composition and regulation of the cellular repertoire of SCF ubiquitin ligases. Cell *171*, 1326–1339.e14. https://doi.org/10.1016/j.cell.2017.10.016.

14. Gutierrez, C., Chemmama, I.E., Mao, H., Yu, C., Echeverria, I., Block, S.A., Rychnovsky, S.D., Zheng, N., Sali, A., and Huang, L. (2020). Structural dynamics of the human COP9 signalosome revealed by cross-linking mass spectrometry and integrative modeling. Proc. Natl. Acad. Sci. USA *117*, 4088–4098. https://doi.org/10.1073/pnas.1915542117.

15. Rozen, S., Füzesi-Levi, M.G., Ben-Nissan, G., Mizrachi, L., Gabashvili, A., Levin, Y., Ben-Dor, S., Eisenstein, M., and Sharon, M. (2015). CSNAP is a stoichiometric subunit of the COP9 signalosome. Cell Rep. *13*, 585–598. https://doi.org/10.1016/j.celrep.2015.09.021.

16. Tomoda, K., Kubota, Y., and Kato, J. (1999). Degradation of the cyclin-dependent-kinase inhibitor p27Kip1 is instigated by Jab1. Nature *398*, 160–165.

17. Dubiel, D., Bintig, W., Kähne, T., Dubiel, W., and Naumann, M. (2017). Cul3 neddylation is crucial for gradual lipid droplet formation during adipogenesis. Biochim. Biophys. Acta. Mol. Cell Res. *1864*, 1405–1412. https://doi.org/10.1016/j.bbamcr.2017.05.009.

18. Bennett, E.J., Rush, J., Gygi, S.P., and Harper, J.W. (2010). Dynamics of cullin-RING ubiquitin ligase network revealed by systematic quantitative proteomics. Cell *143*, 951–965. https://doi.org/10.1016/j.cell.2010.11.017.

19. Emberley, E.D., Mosadeghi, R., and Deshaies, R.J. (2012). Deconjugation of Nedd8 from Cul1 is directly regulated by Skp1-F-box and substrate, and the COP9 signalosome inhibits deneddylated SCF by a noncatalytic mechanism. J. Biol. Chem. *287*, 29679–29689.

20. Wang, J., Dubiel, D., Wu, Y., Cheng, Y., Wolf, D.A., and Dubiel, W. (2021). CSN7B defines a variant COP9 signalosome complex with distinct function in DNA damage response. Cell Rep. *34*, 108662. https://doi.org/10.1016/j.celrep.2020.108662.

21. Schlierf, A., Altmann, E., Quancard, J., Jefferson, A.B., Assenberg, R., Renatus, M., Jones, M., Hassiepen, U., Schaefer, M., Kiffe, M., et al. (2016). Targeted inhibition of the COP9 signalosome for treatment of cancer. Nat. Commun. *7*, 13166. https://doi.org/10.1038/ncomms13166.

22. Milhollen, M.A., Traore, T., Adams-Duffy, J., Thomas, M.P., Berger, A.J., Dang, L., Dick, L.R., Garnsey, J.J., Koenig, E., Langston, S.P., et al. (2010). MLN4924, a NEDD8-activating enzyme inhibitor, is active in diffuse large B-cell lymphoma models: rationale for

treatment of NF-{kappa}B-dependent lymphoma. Blood *116*, 1515–1523.

23. Brownell, J.E., Sintchak, M.D., Gavin, J.M., Liao, H., Bruzzese, F.J., Bump, N.J., Soucy, T.A., Milhollen, M.A., Yang, X., Burkhardt, A.L., et al. (2010). Substrate-assisted inhibition of ubiquitin-like protein-activating enzymes: the NEDD8 E1 inhibitor MLN4924 forms a NEDD8-AMP mimetic in situ. Mol. Cell *37*, 102–111. https://doi.org/10.1016/j.molcel.2009.12.024.

24. Hetfeld, B.K.J., Helfrich, A., Kapelari, B., Scheel, H., Hofmann, K., Guterman, A., Glickman, M., Schade, R., Kloetzel, P.M., and Dubiel, W. (2005). The zinc finger of the CSN-associated deubiquitinating enzyme USP15 is essential to rescue the E3 ligase Rbx1. Curr. Biol. *15*, 1217–1221.

25. Schweitzer, K., and Naumann, M. (2015). CSN-associated USP48 confers stability to nuclear NF-kappaB/RelA by trimming K48-linked Ub-chains. Biochim. Biophys. Acta *1853*, 453–469.

26. Huang, X., Dubiel, D., and Dubiel, W. (2021). The COP9 signalosome variant CSN^{CSN7A} stabilizes the deubiquitylating enzyme CYLD impeding hepatic steatosis. Livers *1*, 116–131. https://doi.org/10.3390/livers1030011.

27. Chaithongyot, S., and Naumann, M. (2022). Helicobacter pylori-induced reactive oxygen species direct turnover of CSN-associated STAMBPL1 and augment apoptotic cell death. Cell. Mol. Life Sci. *79*, 86. https://doi.org/10.1007/s00018-022-04135-2.

28. Huang, X., Wagner, E., Dumdey, R., Peth, A., Berse, M., Dubiel, W., and Berndt, C. (2006). Phosphorylation by COP9 signalosome-associated CK2 promotes degradation of p27 during the G1 cell cycle phase. Isr. J. Chem. *46*, 231–238.

29. Braumann, C., Tangermann, J., Jacobi, C.A., Müller, J.M., and Dubiel, W. (2008). Novel anti-angiogenic compounds for application in tumor therapy - COP9 signalosome-associated kinases as possible targets. Mini Rev. Med. Chem. *8*, 421–428.

30. Zhai, S.S., Ruan, D., Zhu, Y.W., Li, M.C., Ye, H., Wang, W.C., and Yang, L. (2020). Protective effect of curcumin on ochratoxin A-induced liver oxidative injury in duck is mediated by modulating lipid metabolism and the intestinal microbiota. Poult. Sci. *99*, 1124–1134. https://doi.org/10.1016/j.psj.2019.10.041.

31. Abbas, T., Sivaprasad, U., Terai, K., Amador, V., Pagano, M., and Dutta, A. (2008). PCNA-dependent regulation of p21 ubiquitylation and degradation via the CRL4Cdt2 ubiquitin ligase complex. Genes Dev. *22*, 2496–2506.

32. Higa, L.A., Yang, X., Zheng, J., Banks, D., Wu, M., Ghosh, P., Sun, H., and Zhang, H. (2006). Involvement of CUL4 ubiquitin E3 ligases in regulating CDK inhibitors Dacapo/p27Kip1 and cyclin E degradation. Cell Cycle *5*, 71–77. https://doi.org/10.4161/cc.5.1.2266.

33. Huang, X., Ordemann, J., Müller, J.M., and Dubiel, W. (2012). The COP9 signalosome, cullin 3 and Keap1 supercomplex regulates CHOP stability and adipogenesis. Biol. Open *1*, 705–710. https://doi.org/10.1242/bio.20121875.

34. Lee, J.E., Schmidt, H., Lai, B., and Ge, K. (2019). Transcriptional and epigenomic regulation of adipogenesis. Mol. Cell Biol. *39*, e00601-18. https://doi.org/10.1128/MCB.00601-18.

35. Malik, A.U., Karapetsas, A., Nirujogi, R.S., Mathea, S., Chatterjee, D., Pal, P., Lis, P., Taylor, M., Purlyte, E., Gourlay, R., et al. (2021). Deciphering the LRRK code: LRRK1 and LRRK2 phosphorylate distinct Rab proteins and are regulated by diverse mechanisms. Biochem. J. *478*, 553–578. https://doi.org/10.1042/BCJ20200937.

36. Dubiel, D., Gierisch, M.E., Huang, X., Dubiel, W., and Naumann, M. (2013). CAND1-dependent control of cullin 1-RING Ub ligases is essential for adipogenesis. Biochim. Biophys. Acta *1833*, 1078–1084. https://doi.org/10.1016/j.bbamcr.2013.01.005.

37. Bartz, R., Zehmer, J.K., Zhu, M., Chen, Y., Serrero, G., Zhao, Y., and Liu, P. (2007). Dynamic activity of lipid droplets: protein phosphorylation and GTP-mediated protein translocation. J. Proteome Res. *6*, 3256–3265. https://doi.org/10.1021/pr070158j.

38. Guzmán-Ruiz, R., Tercero-Alcázar, C., Rabanal-Ruiz, Y., Díaz-Ruiz, A., El Bekay, R., Rangel-Zuñiga, O.A., Navarro-Ruiz, M.C., Molero, L., Membrives, A., Ruiz-Rabelo, J.F., et al. (2020). Adipose tissue depot-specific intracellular and extracellular cues contributing to insulin resistance in obese individuals. Faseb. J. *34*, 7520–7539. https://doi.org/10.1096/fj.201902703R.

39. Lamber, E.P., Siedenburg, A.C., and Barr, F.A. (2019). Rab regulation by GEFs and GAPs during membrane traffic. Curr. Opin. Cell Biol. *59*, 34–39. https://doi.org/10.1016/j.ceb.2019.03.004.

40. Akopian, D., McGourty, C.A., and Rapé, M. (2022). Co-adaptor driven assembly of a CUL3 E3 ligase complex. Mol. Cell *82*, 585–597.e11. https://doi.org/10.1016/j.molcel.2022.01.004.

41. Lin, H., Yan, Y., Luo, Y., So, W.Y., Wei, X., Zhang, X., Yang, X., Zhang, J., Su, Y., Yang, X., et al. (2021). IP6-assisted CSN-COP1 competition regulates a CRL4-ETV5 proteolytic checkpoint to safeguard glucose-induced insulin secretion. Nat. Commun. *12*, 2461. https://doi.org/10.1038/s41467-021-22941-3.

42. Berndt, N., Eckstein, J., Heucke, N., Gajowski, R., Stockmann, M., Meierhofer, D., and Holzhutter, H.G. (2019). Characterization of lipid and lipid droplet metabolism in human HCC. Cells *8*. https://doi.org/10.3390/cells8050512.

43. Shi, J., Hua, X., Zhu, B., Ravichandran, S., Wang, M., Nguyen, C., Brodie, S.A., Palleschi, A., Alloisio, M., Pariscenti, G., et al. (2016). Somatic genomics and clinical features of lung adenocarcinoma: a retrospective study. PLoS Med. *13*, e1002162. https://doi.org/10.1371/journal.pmed.1002162.

44. Huang, X., Ordemann, J., Pratschke, J., and Dubiel, W. (2016). Overexpression of COP9 signalosome subunits, CSN7A and CSN7B, exerts different effects on adipogenic differentiation. FEBS Open Bio *6*, 1102–1112. https://doi.org/10.1002/2211-5463.12129.

STAR★METHODS

KEY RESOURCES TABLE

REAGENT or RESOURCE	SOURCE	IDENTIFIER
Antibodies		
Actin	Santa Cruz	sc-47778
Caveolin 1	Abcam	ab2910
CSN1	ENZO life science	BML-PW8285
CSN2	Abcam	ab155774
CSN3	Abcam	ab79698
CSN5(JAB1)	GeneTex	GTX70207
CSN7A	Santa Cruz	sc-398882
CSN7A	Abcam	ab235400
CSN7B	Abcam	ab124718
CUL-1	Santa Cruz	sc-12761
CUL-3 WB, IF	BD biosciences	611848
CUL-3 IP, IF	Bethyl Laboratories	A301-109A
CUL4A for WB	Abcam	ab92554
CUL4A for IP	Abcam	ab72548
CUL4B for IP	Abcam	ab227724
CUL4B	Abcam	ab67035
FLAG M2	Sigma	F-1804
GAPDH	Millipore	MAB374
GST	Santa Cruz	sc-53909
HA-probe (Y-11)	Santa Cruz	sc-805
LAMIN B	Santa Cruz	sc-133722
C23	Santa Cruz	sc-13057
PPAR-γ	Cell signaling	#2443S
p53 (DO-1)	Santa Cruz	sc-126
p27	Cell Signaling	#3698
p21	Cell Signaling	#2946
RAB18	Sigma	SAB4200173
USP15 for WB	Abnova	H00009958-M1
USP15 for IP	Enzo life sciences	BML-PW9795
USP48	Abcam	ab72226
γ-Tubulin	Santa Cruz	sc-17787
Chemicals, beads, and recombinant proteins		
CSN5i-3	Novartis	SB-58-SN29
Curcumin	Sigma	C1386-5G
MLN4924	MedChemExpress	HY-70062
MG132	Selleckchem	S2619
FLAG peptide	Sigma Aldrich	F3290
Anti-FLAG M2 affinity gel	Sigma Aldrich	A2220
Protein A Sepharose	GE Health Care	170780–01
HRP-secondary antibodies	Santa Cruz	sc-2005, sc-2004

(*Continued on next page*)

Continued

REAGENT or RESOURCE	SOURCE	IDENTIFIER
Secondary FITC-antibodies	Life Technologies	A11072; A11017,
Cy3	Dianova	711-165-152
Alexa 643	Dianova	715-605-151
Chemiluminescent substrate	Millipore	WBKLS0500
GST-p27	Abnova	H00001027
GST-RAB18	Abnova	H00022931
GST-CAV1	Abnova	H00000857
Oligonucleotides, plasmids, and recombinant proteins		
siRAB18: 5′-3′GGA AGA AGG CCA AGG AGG AUU	Eurofins	Customer siRNA
For generation of plasmid: FLAG-CSN7A$^{1-200}$ 5′-3′ AACCAACACAAGGAGTAGC AGCTGGGCCTG	Eurofins	Customer oligonucleotides
For generation of plasmid: FLAG-CSN7B$^{1-200}$ 5′-3′ AACCAGTACAAAGAGTAA CCACAACCGAAC	Eurofins	Customer oligonucleotides
CSN7A CRISPR/Cas9 KO plasmid	Santa Cruz	sc-408503
CSN7B CRISPR/Cas9 KO plasmid	Santa Cruz	sc-408275
FLAG-CSN7A eukaryotic plasmid	This paper	N/A
FLAG-CSN7B eukaryotic plasmid	This paper	N/A
FLAG-CSN7A$^{1-200}$ eukaryotic plasmid	This paper	N/A
FLAG-CSN7B$^{1-200}$ eukaryotic plasmid	This paper	N/A
HA-FLAG-USP15	Addgene	#22570
FLAG-CSN5	This paper	N/A
EGFP-RAB18	Addgene	#49550
FLAG-CSN1-8 procaryotic plasmids	[27]	N/A
GFP-CSN7A eukaryotic plasmid	This paper	N/A
Commercial kits		
FITC Annexin V Apoptosis Detection Kit	Mab Tag	AnxF100PI
Purexpress *in vitro* protein synthesis kit	NEW England BioLabs	#E6800
QuikChange II XL site directed mutagenesis kit	Agilent Technologies	#200521-5
Experimental Models: Cell Lines		
MRC5	ATCC	CCL-171
AD293	ATCC	CRL-1573
AD293-FLAG-CSN7A	This paper	N/A
AD293-FLAG-CSN7B	This paper	N/A
HeLa-*CSN7A*-KO	This paper	N/A
HeLa-*CSN7B*-KO	This paper	N/A
LiSa-2-CSN7A-KD	This paper	N/A
LiSa-2-*CSN7B*-KO	This paper	N/A
LiSa-2-FLAG	This paper	N/A
LiSa-2-FLAG-CSN7A	This paper	N/A
LiSa-2-FLAG-CSN7B	This paper	N/A
LiSa-2-FLAG-CSN7A$^{1-200}$	This paper	N/A
LiSa-2-FLAG-CSN7B$^{1-200}$	This paper	N/A
LiSa-2-GFP-CSN7A	This paper	N/A

(*Continued on next page*)

Continued

REAGENT or RESOURCE	SOURCE	IDENTIFIER
Software		
DIVA software 9.1	BD Biosciences	https://www.bdbiosciences.com/en-us/products/software
LASX	Leica Mannheim, Germany	https://www.leica-microsystems.com/de/produkte/mikroskop-software/p/leica-las-x-ls/
GraphPad Prism 8.0.1	GraphPad Software, Inc	https://www.graphpad.com/scientific-software/prism/

RESOURCE AVAILABILITY

Lead contact

Further information and requests for resources and reagents should be directed to and will be fulfilled by the lead contact, Wolfgang Dubiel (wolfgang.dubiel@med.ovgu.de).

Materials availability

All reagents generated in this study are available from the lead contact with a completed Materials Transfer Agreement. We are glad to share all reagents with compensation by requestor for shipping.

Data and code availability

- All data reported in this paper will be provided by the lead contact upon request.
- This paper does not contain original code.
- Additional information required to reanalyze the data reported in this paper is available from the lead contact.

EXPERIMENTAL MODEL

Studies were performed with *CSN7A* or *CSN7B* knockout HeLa cells called HeLa-*CSN7A*-KO and HeLa-*CSN7B*-KO cells or with CSN7A KD and *CSN7B* KO LiSa-2 cells called LiSa-2-CSN7A-KD or LiSa-2-*CSN7B*-KO cells. HeLa and LiSa-2 derived cells were grown in 5% CO_2 humidified incubator at 37°C in DMEM medium supplemented with 10% FBS, 100 U/ml penicillin. AD293 and LiSa-2 cells stably expressing FLAG, FLAG-CSN7A, FLAG-CSN7B, FLAG-CSN7A$^{1\text{-}200}$ and FLAG-CSN7B$^{1\text{-}200}$ were grown in the same medium supplemented with 0.5 mg/mL G418. HeLa or LiSa-2 cells in which *CSN7A* or *CSN7B* were disrupted by CRISPR/Cas9 gene editing were grown in IMDM or DMEM medium supplemented with 0.5 mg/mL G418. LiSa-2 cells stably transfected with GFP-CSN7A were generated as described before.[20]

METHOD DETAILS

Plasmid transfections and stable cell lines

Generation of FLAG, FLAG-CSN7A and FLAG-CSN7B plasmids[44] and of GFP-CSN7A[20] was described. Truncated versions FLAG-CSN7A$^{1\text{-}200}$ and FLAG-CSN7B$^{1\text{-}200}$ were obtained by insertion of stop-codons using site directed mutagenesis kit (Agilent Technologies) according to the manufacturer's protocol.

To generate stable transfectants, plasmids were transfected using Lipofectamine 2000 (Life Technologies) according to the manufacturer's protocol. After transfection, cells permanently expressing FLAG, FLAG-CSN7A, FLAG-CSN7B, and their truncated versions and GFP-CSN7A derived from AD293 or LiSa-2 cells, were selected with 0.5 mg/mL G418 for 1 to 3 weeks. Individual clones were isolated and propagated in the selection medium. To establish *CSN7A* and *CSN7B* knockout cell lines following CRISPR/Cas9 manipulations as described,[20] LiSa-2 or HeLa derived cells were grown in medium containing 0.5 mg/mL G418 for 2 or 3 weeks.

RNA interference

Transfection of siRNAs against GFP (control) and RAB18 was conducted using Lipofectamine 2000 transfection reagent (Life Technologies) according to manufacturer's protocol. siRNAs were transfected into LiSa-2 cells at a final concentration of 50 nM of siRNA, 48 h before further experiments.

Protein extraction, immunoblotting and immunoprecipitation

Whole cell lysates were prepared in triple-detergent buffer (50 mM Tris-HCl, pH 8.5, 150 mM NaCl, 0.02% (w/v) sodium azide, 0.1% (w/v) SDS, 1% (v/v) NP-40, 0.5% (w/v) sodium deoxycholate) described before.[17] Samples were subjected to denaturing 10% or 12.5% SDS-PAGE and transferred onto 0.2 μm PVDF membranes. Transfer to the membrane was controlled by Ponceau Red staining, and membranes were blocked with 5% milk in TBS containing 0.1% Tween 20 for 1 h. Membranes were incubated with appropriate antibodies overnight at 4°C and were washed three times for 5 min with TBST, followed by incubation with HRP-conjugated secondary antibodies for 1 h at room temperature. Blots were washed three times for 5 min with TBST and incubated with chemiluminescent substrate and respective protein bands were visualized using the ChemoCam Imager (Intas, Germany).

For immunoprecipitation protein extracts were prepared in mono-detergent TBS buffer (50 mM Tris-HCl, pH 7.4, 150 mM NaCl, 1 mM EDTA, pH 8.0, 1% Triton X-100) described previously.[17] Cellular debris was removed by centrifugation for 10 min at 13.000 × rpm and 4°C. Supernatants were incubated with appropriate antibodies using 1–5 μg for 2 h at 4°C. Pre-washed Protein-A Sepharose was added, and the mixture was rotated overnight at 4°C. Beads were washed three times with lysis buffer and boiled with 2x Laemmli SDS-PAGE sample buffer. Immunocomplexes were separated on SDS-PAGE and analyzed by immunoblotting with indicated antibodies.

FLAG pulldowns

AD293 and LiSa-2 cells with FLAG-tagged CSN7A or CSN7B paralogs were lyzed in mono-detergent buffer described above. Cell lysates were subjected to the pre-equilibrated ANTI-FLAG M2 affinity column (Sigma, St. Louis, MO, USA). After washing with 20 column volumes of mono-detergent buffer, bound proteins were eluted by competition with the FLAG peptide of 100 μg/mL as recommended by the manufacturer's protocol. Proteins were separated on SDS-PAGE and analyzed by immunoblotting using indicated antibodies.

Subcellular fractionation

Subcellular fractionation was performed as described.[27] Cells were lysed in buffer A (20 mM Tris/HCl, pH 7.9, 10 mM NaCl, 1.5 mM $MgCl_2$, 10 mM K_2HPO_4, 10% glycerol supplemented with 0.5 mM AEBSF, 1 mM sodium orthovanadate, 1 mM sodium molybdate, 10 mM sodium fluoride, 20 mM 2-phosphoglycerate and protease inhibitor mix (Roche Germany)). After addition of NP-40 at a final concentration of 0.125%, the cytosolic fraction was obtained by centrifugation at 13000 × g for 10 min at 4°C. The nuclear pellet was resolved in buffer C (20 mM Tris/HCl, pH 7.9, 420 mM NaCl, 1.5 mM $MgCl_2$, 10 mM K_2HPO_4, 10% glycerol, 0.2 mM EDTA supplemented with the same inhibitors as before). The sample was incubated for 15 min on ice and centrifuged for 10 min at 13 000 × g *at 40C*. The insoluble nuclear fraction was achieved by digesting the resulting pellet with 1 μL nuclease (Calbiochem, Germany) in buffer E (20 mM Tris/HCl, pH 7.8, 150 mM NaCl, 1.5 mM $MgCl_2$, 5 mM $CaCl_2$, 10% glycerol supplemented with the same inhibitors as before) at 4 °C for 30 min. After centrifugation at 13000 x *g* for 10 min at 4°C the supernatants were used as N2 (insoluble nuclear) fraction.

In vitro and cell binding assays

For *in vitro* binding assay, human FLAG-tagged CSN subunits were translated in procaryotic system using translation kit and incubated with different recombinant GST-tagged proteins for 1 h at 37°C. After incubation, immunoprecipitations with 2 μg GST antibody were performed as described before.[27]

For binding assays in HeLa cells, co-transfections with 6 μg of appropriate plasmids indicated in Figures 2C and 2D were performed. After 16 h, cells were collected and lysed in mono-detergent buffer described above. Supernatants were separated from cell debris by centrifugation and incubated with 2–5 μg of indicated antibodies for immunoprecipitations. After immunoprecipitation, precipitates from *in vitro* and cell binding assays were subjected to SDS-PAGE and analyzed with indicated antibodies.

Curcumin-induced apoptosis and monitoring by flow cytometry analysis

Apoptosis in HeLa derived cells was induced by 12.5, 25, and 50 μM of curcumin and after 12 h analyzed by immunoblotting with indicated antibodies (Figure 3A). In another experiment, HeLa derived cells were pre-incubated with MLN4924 (1 μM), CSN5i-3 (1 μM) and MG132 (10 μM) for 2 h and then incubated for another 10 h with 50 μM curcumin and analyzed by immunoblotting with the same antibodies (Figure S1F).

For flow cytometry analysis, HeLa-WT, HeLa-*CSN7A*-KO, and HeLa-*CSN7B*-KO cells without or with 50 μM curcumin treatment were collected after 18 h. For rescue experiment, HeLa derived cells with different CSN7A and CSN7B backgrounds were transfected with 2 μg plasmid of FLAG-vector (control), FLAG-CSN7B and FLAG-CSN7B$^{1\text{-}200}$. After 4 days of transfection, cells were treated with 50 μM curcumin for 12 h. After drug exposure, cells were stained. Annexin V staining was performed with the FITC Annexin V Apoptosis Detection Kit. Cells (1×10^6 cells) were trypsinized, washed twice with cold PBS, and resuspended to 90 μL buffer. Fife μl FITC-conjugated anti-Annexin V and 5 μL propidium iodide (PI) (0.5 μg/mL) were added. Cells were gently vortexed, followed by incubation for 20 min at room temperature in the dark. Samples were measured by the flow cytometer LSR-Fortessa (BD Biosciences, USA). Data were analyzed using DIVA software version 9.1.

Adipogenesis and ORO staining

Adipogenesis in LiSa-2 derived cells with CSN7A KD and *CSN7B* KO or stably expressed FLAG-tagged CSN7 paralogs or truncated FLAG-tagged CSN7 paralogs LiSa-2-FLAG-CSN7A$^{1\text{-}200}$ and LiSa-2-FLAG-CSN7B$^{1\text{-}200}$ was induced for 1, 8, and 15 days by culturing cells in serum-free medium with supplements including 1 nM insulin, 20 p.m. triiodothyronine and 1 mM cortisol, which was changed every 2 days[33] Formation of lipids was determined by ORO staining, visualized by light microscopy and quantified spectrophotometrically at 520 nm as described before.[44]

Immunostaining and confocal fluorescence microscopy

LiSa-2 cells with different backgrounds were exposed to adipogenic differentiation for 15 days in chamber slides. After differentiation, cells were washed three times with PBS and fixed in 4% paraformaldehyde for 15 min. Fixed samples were permeabilized with 0.1% Triton X-100/PBS for 10 min at room temperature and blocked with 5% filtered BSA in PBS for 1 h. Samples were incubated with primary antibodies directed against CUL3 (mouse), RAB18 (rabbit), CSN7A (rabbit) or CSN7B (rabbit) in indicated combinations in 5% BSA in PBS overnight at 4°C. Thereafter, samples were washed three times in PBS, and stained for 1 h at room temperature with secondary antibodies coupled to Alexa Fluor 488 (anti-mouse), Alexa Fluor 594 (anti-rabbit), Alexa Fluor 647 (anti-mouse), Cy3 (anti-rabbit) fluorophores with 5% BSA in PBS. Nuclei were counterstained using DAPI. Slides were analyzed and visualized using qan inverted confocal microscopy system Leica SP8 (Leica Mannheim, Germany) equipped with a Plan Apo 63x/1.4 oil objective and controlled by LASX software (Leica Mannheim, Germany). To circumvent bleed-through between the three spectral channels, sequential unidirectional scanning was performed at 600 Hz using the following settings: sequence 1: excitation 405 nm + 561 nm, emission 435–475 nm and 605–660 nm combined with transmitted light detection; sequence 2: excitation 488 nm, emission 510–565 nm; sequence 3: excitation 550 nm, emission 569 nm; and sequence 4: excitation 652 nm, emission 671 nm. Sequences were altered between lines and voxel size was adjusted to 80 nm × 80 nm × 300 nm (dx, dy, dz). Images of the individual channels were pseudo colored: DAPI (excitation 405 nm) in blue, Alexa Fluor 488 (excitation 488 nm) in green or red, Alexa Fluor 594 (excitation 561 nm) in red, Alexa Flour 647 (excitation 652 nm) in red, and Cy3 (excitation 550 nm) in magenta. DAPI (excitation 405 nm) in blue, Alexa Fluor 488 (excitation 488 nm) in green and Alexa Fluor 594 (excitation 561 nm) in red. Single planes out of the data stacks were analyzed using ImageJ software and localization of different proteins were represented with different colors.

QUANTIFICATION AND STATISTICAL ANALYSIS

ImageJ software was used to quantify SDS-PAGE protein bands visualized by ChemoCam Imager (Intas, Germany). Statistics were calculated with GraphPad Prism 8.0.1 software. Error bars represent standard deviations (SD). For statistical analysis unpaired Student's *t* test was used. Number n represents the number of independent experiments. *p* values of $p < 0.05$ were considered statistically significant. Statistical details of individual experiments can be found in the figure legends.